

# Flow Past a Cylinder using Lattice Boltzmann Method

A Thesis Submitted to  
Indian Institute of Technology Hyderabad  
in partial fulfillment of the  
requirements for the Degree of

**MASTER OF TECHNOLOGY**

in  
Faculty of Engineering

by

**Ashima Sehgal**



भारतीय प्रौद्योगिकी संस्थान हैदराबाद  
Indian Institute of Technology Hyderabad

DEPARTMENT OF CHEMICAL ENGINEERING  
INDIAN INSTITUTE OF TECHNOLOGY HYDERABAD  
Hyderabad – 502 205

MAY 2014



*To my parents and brother*



## DECLARATION

I declare that this written submission represents my ideas in my own words, and where ideas or words of others have been included, I have adequately cited and referenced the original sources. I also declare that I adhered to all principles of academic honesty and integrity and have not misrepresented or fabricated or falsified any idea/data/fact/source in my submission. I understand that any violation of the above will be cause for disciplinary action by the Institute and can also evoke penal action from the sources that have thus not been properly cited, or from whom proper permission has not taken when needed.

*Ashima Sehgal*

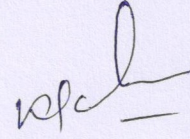
---

Ashima Sehgal

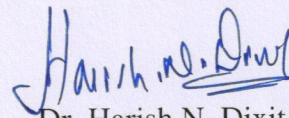


APPROVAL SHEET

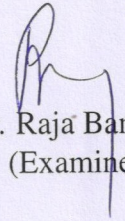
This thesis entitled Flow over a cylinder using lattice Boltzmann method by Ms. Ashima Sehgal is approved for the degree of Master of Technology from IIT Hyderabad.



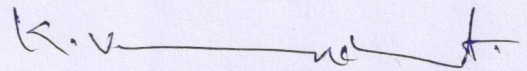
Dr. Kirti Chandra Sahu  
( Research Supervisor)



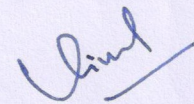
Dr. Harish N. Dixit  
( Research Co-supervisor)



Dr. Raja Banerjee  
(Examiner)



Dr. K. Venkatasubbaiah  
(Examiner)



DR. VINOD JANARDHANAN  
(INTERNAL EXAMINER)





## Acknowledgements

*This thesis would not have been completed without the help, inspiration and advise of many individuals. Some of the names I might forget to mention here but each one of them have played a role in fulfillment of this work.*

*First and foremost, I am forever indebted to Dr. Kirti Chandra Sahu, my advisor, and Dr. Harish Dixit, my co-advisor for motivating and guiding me along this memorable journey. They remains and will remain, first source of advice and a constant source of inspiration, both in research and in life. They are the fist ones in my life who taught me the alphabets of research. The numerous discussions I had with them in their offices are the priceless lectures for which I will remain ever grateful to them.*

*I am very much thankful to our Director, Prof. U. B. Desai, for providing us with an environment to carry out our research without any hurdles.*

*I would like to express my sincere gratitude to our Head of the Department, Dr. Vinod Janarthanan, who support us in every possible way for the completion of this project.*

*I am very much grateful to all the members of my committee, Dr. Raja Banerjee and Dr. venkatsubhaiya, for their invaluable suggestion which helped me enormously during this work.*

*I would like to thank all the faculty members of Department of Chemical Engineering, IIT Hyderabad, for their unforgettable encouragement.*

*I would like to thank all my M.Tech and PhD colleagues for helping me one way or another during the project. I would like to express my special thanks to my PhD colleague Manoj Kumar Tripathi for making me familiar with “tecplot”, “latex”, “gerris”, “xmgrace”, and many other essential tools.*

*Finally, I would like to express my deepest of gratitude towards my parents for the unconditional love and support they have given me through out my life. I take this opportunity to thank my brother, Puneet, without their love and encouragement, I would not have been able to come to this place.*



## Synopsis

In this thesis, an oscillatory flow over a rectangular cylinder has been investigated by varying the amplitude and frequency of the imposed flow. The region without reverse flow at the inlet of the computational domain is only considered. The objective of this thesis is to understand the formation of different vortex shedding modes and the transition from one mode to another as the frequency and amplitude ratio are varied. A lattice Boltzmann method is used in order to simulate this problem with non-uniform meshes. The problem considered in the thesis is an extremely difficult problem computationally as in order to get any accurate solution one has to use very fine mesh near the cylinder. In order to overcome this difficulty, a non-uniform mesh has been used in the present LBM solver. For frequency ratio 0.7, it is found that for lower amplitude ratio the vortex-shedding pattern is antisymmetrical; for intermediate amplitude ratio chaotic mode is observed and symmetric shedding is found for higher amplitude ratio. For a fixed amplitude ratio 0.1, and varying the frequency ratio, we have not observed much difference in vortex shedding mode. Thus for getting different vortex shedding mode, one has to vary amplitude ratio's. Hence probability of getting symmetric modes is for low frequency ratio and for a high range of amplitude ratio.



## List of Figures

1.1	Schematic showing the behaviour of fluid at different $Re$ , Reynolds number, when a body is kept stationary in a uniform flow. . . . .	3
1.2	Schematic showing vorticity generated at the surface of cylinder . . . . .	4
2.1	Schematic showing the actual problem (which we want to study) and the analogous problem (which we have modeled) . . . . .	11
2.2	Schematic showing the geometry (not to scale) with an oscillating inlet at $x = 0$ . . . . .	12
2.3	Schematic showing the non-uniform grid. . . . .	12
2.4	Schematic streaming and collision at each time step. . . . .	13
2.5	$D2Q9$ model . . . . .	15
3.1	Schematic showing the region of interest for the defined problem, with no reverse flow (not to scale). . . . .	19
3.2	Contours of the vorticity for a square cylinder,(a) 80 points per unit length on the body surface, (b) 120 points per unit length on the body surface, (c) 160 points per unit length on the body surface. The rest of the parameters are $Re = 100$ , $f_r = 2$ , $a_r = 0.5$ . . . . .	20
3.3	Contours of the vorticity,(a) $300 \times 300$ , (b) $400 \times 400$ , (c) $500 \times 500$ . The rest of the parameters are $Re = 100$ , $f_r = 2$ , $a_r = 0.5$ . . . . .	21
3.4	(a) Graph showing the power spectrum obtained from the code for the calculation of Strouhal number, $St$ for the non-oscillating square cylinder and (b) variation of Strouhal number, $st$ with Reynolds number, $Re$ as found by Okajima (1982). Shown in the red are the Strouhal number obtained from our code and in blue dot from gerris. . . . .	22

- 3.5 Schematic showing the contours of the vorticity for a square cylinder, which is showing different vortex shedding pattern with phase plots at different points in the domain. The parameters are Reynolds number,  $Re = 100$ , frequency ratio,  $f_r = 0.7$ , amplitude ratio: a)  $a_r = 0.1$  b)  $a_r = 0.5$ , c)  $a_r = 1.1$ , d)  $a_r = 1.65$ . . . 24
- 3.6 Schematic showing the contours of vorticity for a square cylinder along the yellow dotted line, as shown in figure 3.1 . The parameters are Reynolds number,  $Re = 100$  The values for frequency and amplitude ratio's are: a)  $f_r = 1, a_r = 0.1$  b)  $f_r = 2, a_r = 0.1$ , c)  $f_r = 3, a_r = 0.1$ , d)  $f_r = 4, a_r = 0.1$ ,  $f_r = 5, a_r = 0.1$  . . . . 25
- 3.7 Schematic showing the contours of vorticity, for a rectangular cylinder for the borderline cases as shown in figure 3.1 . The parameters are Reynolds number,  $Re = 200$  The values for frequency and amplitude ratio's are: a)  $f_r = 1, a_r = 0.8$  b)  $f_r = 2, a_r = 0.4$ , c)  $f_r = 3, a_r = 0.26$ , d)  $f_r = 4, a_r = 0.2$ ,  $f_r = 5, a_r = 0.16$  . . . . 26

# Contents

<b>Acknowledgements</b>	<b>v</b>
<b>Synopsis</b>	<b>vii</b>
<b>List of Figures</b>	<b>x</b>
<b>1 Introduction</b>	<b>1</b>
1.0.1 Focus of the present study . . . . .	2
1.0.2 Motivation for the work . . . . .	2
1.0.3 How does the flow occur? . . . . .	3
1.0.4 Shedding modes for an oscillating cylinder . . . . .	3
1.0.5 Effect of geometry . . . . .	4
1.0.6 Effect of Boundary conditions . . . . .	5
1.0.7 Effect of oscillations . . . . .	6
1.0.8 Structure of the thesis . . . . .	8
<b>2 Formulation</b>	<b>11</b>
2.1 Numerical method . . . . .	13
2.1.1 Introduction to lattice Boltzmann method . . . . .	13
2.1.2 D2Q9 model . . . . .	14
2.1.3 Calculation of variables . . . . .	15
2.1.4 Boundary conditions . . . . .	16

2.2	Dimensionless numbers . . . . .	17
<b>3</b>	<b>Results and discussion</b>	<b>19</b>
3.1	Results obtained from lattice Boltzmann method . . . . .	20
3.1.1	Grid Independence Test . . . . .	20
3.1.2	Domain independence test . . . . .	21
3.1.3	Comparison with the literature . . . . .	22
3.1.4	Antisymmetric to symmetric mode . . . . .	23
3.1.5	(a) Varying amplitude ratio . . . . .	23
3.1.6	(b) Varying frequency ratio . . . . .	25
3.1.7	Varying frequency ratio and amplitude ratio simultaneously . . . . .	26
<b>4</b>	<b>Concluding remarks</b>	<b>27</b>
	<b>Appendices</b>	<b>29</b>
<b>I</b>	<b>Navier-Stokes equation from the Boltzmann equation</b>	<b>29</b>
.1	Proof of Eq. (I.2) . . . . .	29
.2	Proof of Eq. (I.3) . . . . .	30
.3	Proof of Eq. (I.4) . . . . .	31
.4	Proof of Eq. (I.5) . . . . .	32
.5	Proof of Eq. (I.6) . . . . .	33
A	Moments of Maxwell-Boltzmann equilibrium distribution function . . . . .	35
A.1	Zeroth moment of equilibrium distribution function . . . . .	35
A.2	First moment of equilibrium distribution function . . . . .	35
A.3	Second moment of equilibrium distribution function . . . . .	36
A.4	Third moment of equilibrium distribution function . . . . .	36
B	Conservation of mass . . . . .	37
C	Conservation of momentum . . . . .	37



**Bibliography**



# CHAPTER 1

## Introduction

Flow past a cylinder is a very interesting problem which has been studied extensively by several researchers experimentally and numerically. It has many industrial applications like in structural designing, aerodynamics, wind engineering and electronics cooling. In everyday life, we see several examples of flow past rectangular, circular or other irregularly shaped objects like air flow past buildings, skyscrapers and buses, water flow past dams and bridge supporting structures, soup flowing past beans and carrot pieces, and computer fan blowing air past the electronic circuits. A thorough understanding of these kind of flows is very important and sometimes even critical to the performance of many real life systems and processes, as is obvious from the examples cited here. These kinds of flows may be steady or unsteady, which may generate a constant or a time-varying force on the body, respectively. One such example is uniform flow past a rectangular cylinder, for which the flow becomes unsteady above  $Re \approx 40$ . Creating a variable force on the body (Cylinder which is kept in a uniform flow) flow dynamics, is also important in determining the characteristics, acoustics as well as the structural integrity of the system.

It might come as a surprise to a naiver fluid-mechanician, that an initially symmetric (about a plane parallel to the incoming flow direction) flow past a body may become strongly asymmetric as the Reynolds number is increased, where Reynolds number is based on the mean inlet velocity, body size and the viscosity of the fluid. As shown in the figure 1.1, the body seems to shed vortices in the flow direction periodically, above a certain Reynolds number. When the flow becomes oscillatory, it may match the natural frequency of the body and generate destructive, high amplitude vibrations. This is the reason for singing of stationary wires in wind [Relf & Simmons 1925]. In some cases, the incoming flow itself could be oscillatory, which is the central topic of our study, and it has been found by several researchers that the dynamics of such flows can vary from its uniform counter part. Such flows may give rise to different kinds of vortex shedding modes at different frequency ( $f_r$ ) and amplitude ratios ( $a_r$ ), where  $f_r$  is the frequency ratio which is defined as the ratio of frequency of oscillation to the natural vortex shedding frequency for an non oscillating case and  $a_r$  is the amplitude ratio which is defined as the ratio of amplitude of oscillation to the height of the rectangular cylinder. It is important to note that for a uniform flow past stationary cylinder, the vortex shedding mode has been observed to be antisymmetric for any body.

### 1.0.1 Focus of the present study

Generally flow past a structure has similar instabilities irrespective of its shape, whether it is rectangle or circle or any other shape but the boundary layer separation mechanism is significantly different. The flow dynamics is very much dependent on the geometry of the body. For example the vortex formation region is significantly broader and longer for a square cylinder as compared to a circular cylinder because of a larger effective surface area in the wake side of a square cylinder. In the present study, our focus is to understand the formation of different shedding modes and the transition from one mode to another as the frequency and amplitude is varied. The basic mechanism of formation of these different modes is shown in the figure 1.2. As discussed by Xu *et al.* (2006), the flow past an oscillating cylinder can be thought of as a combination of flow past a stationary cylinder and an oscillating cylinder in a stationary fluid. As expected, flow past a stationary cylinder would give rise to antisymmetric shedding of vortices for a sufficiently high  $Re$ , whereas an oscillating cylinder in a stationary fluid would generate a pair of symmetric vortices at top and bottom of the cylinder, simultaneously. If the flow is able to convect these symmetric pairs of vortices away from the cylinder, we get a symmetric mode of vortex shedding. In another scenario, if the frequency or the amplitude of oscillation is not enough to generate and shed sufficiently strong symmetric vortices, the antisymmetric shedding takes place. Alternatively, if the Reynolds number is enough to shed antisymmetric vortices and the oscillation frequency and amplitude is enough to produce sufficiently strong symmetric vortices, a mixed mode appears, which is a combination of the two modes. Thus, we see that the flow past an oscillating cylinder can result in several vortex shedding modes.

### 1.0.2 Motivation for the work

Neglecting the flow dynamics past bodies may result in poor performance of the system or in worst cases it may even lead to disasters like the Tacoma Narrows Bridge collapsed that happened in 1940. The Tacoma Narrows Bridge was the first suspension bridge in the U.S. state of Washington that spanned the Tacoma Narrows strait of Puget Sound between Tacoma and the Kitsap Peninsula. It opened to traffic on July 1, 1940, and dramatically collapsed on November 7, 1940. This bridge fell down due to the effects of resonance. Resonance is the tendency of a structure to respond at an increased amplitude when the frequency of its oscillation matches its natural frequency of vibration. In this case, due to high speed of air which is blowing at 45 kmph, natural frequency of the bridge matched with the vortex shedding frequency and then bridge started oscillating in the vertical direction. As the vibrations became more and more violent, the stresses crossed the maximum load limit, resulting in the collapse of the bridge.

Not always does the ignorance of vortex shedding lead to tragedies, but it does affect the performance or efficiency of the systems involving fluid flows at Reynolds numbers in the regime where vortex shedding may take place. For instance, airplane and glider wings may flutter due to the vortex shedding and it is important to take care of the geometry and the material of the component to avoid a match with the shedding frequency. On the other hand, sometimes it may be desirable to allow vortex shedding. Vortex shedding frequency is mea-

sured in Vortex shedding flow meters to measure the flow rate. Also, it is desirable in waving flags and decorative papers in front of a fan.

The different modes are important to study because they can generate different kind of forces on the body. As discussed earlier, antisymmetric mode of shedding would lead to an oscillatory lift and drag on the body which may not be desirable. On the other hand, a symmetric mode of shedding would generate symmetric forces at the top and bottom of the body, which does not produce any transverse oscillations. Although it is a great result that merely by changing the  $f_r$  and  $a_r$ , we can stop the transverse oscillations of a body, the author is not aware of any applications currently.

### 1.0.3 How does the flow occur?

The motion of the fluid over a rectangular cylinder strongly depends upon aspect ratio (height to width of the cylinder), blockage (width of the cylinder to the domain width), Reynolds number, surface roughness, end conditions and orientation of the body. It is well known fact that as the Reynolds number increases, a sequence of complex events takes place. For a fixed body, at a low Reynolds number, flow smoothly divides and then reunites around the body. At a Reynolds number approximately in between 3.2 to 6 Homann (1936); Nisi & Porter (1923); Taneda (1956), wake bubble forms behind the body. This wake bubble is not a stable structure and it keeps on changing its shape due to increase in Reynolds number. As the Reynolds number reaches approximately a value in between 30 to 40 Goldstein & Rosenhead (1936); Homann (1936); Kovasznay (1949); Roshko (1954), wake bubble bursts and the eddies which it contains, start convecting with the flow. As the Reynolds number crosses a value of 40 approximately, it starts convecting vortices in an alternating manner i.e. one from the top and another from the bottom alternately. This phenomenon of convection of eddies with the flow is called as vortex shedding.

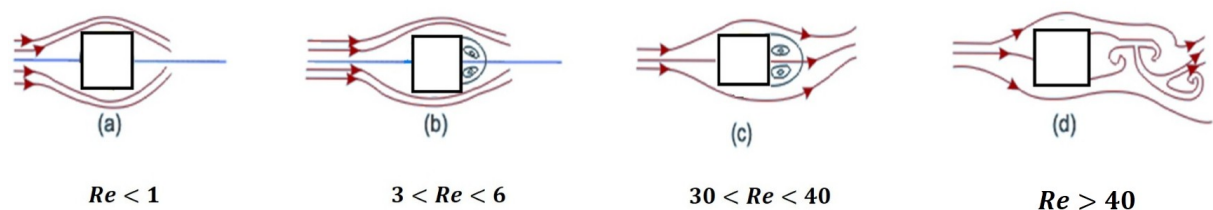


**Figure 1.1:** Schematic showing the behaviour of fluid at different  $Re$ , Reynolds number, when a body is kept stationary in a uniform flow.

### 1.0.4 Shedding modes for an oscillating cylinder

An oscillating cylinder in a uniform flow can be considered as a combination of a cylinder which is oscillating in a fluid kept at rest and a stationary cylinder kept in a uniform flow

Xu *et al.* (2006). When the cylinder is stationary and kept in a uniform flow, and the wake region become unstable, it starts shedding vortices in an alternating manner i.e. one from the top and another from the bottom of the cylinder alternately. As shown in the first panel of the figure (1.2), for a stationary cylinder in a uniform flow, the vorticity generation about the horizontal axis is anti-symmetrical. However, as shown in the second panel of the same figure, the vorticity is generated symmetrically at the surface of the cylinder, about the horizontal axis (which passes through the center of the cylinder). Combination of the above two situations at different amplitude ratio and frequency ratio will result in different types of shedding modes which have been discussed in detail in the results section.

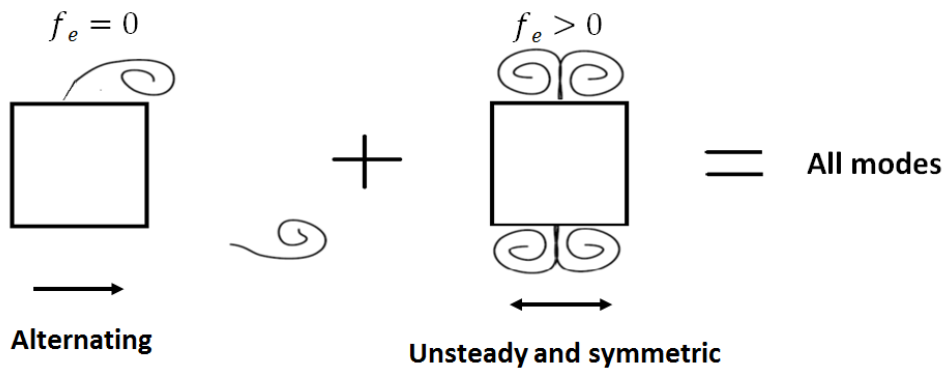


**Figure 1.2:** Schematic showing vorticity generated at the surface of cylinder

As described earlier in the text, flow past a cylinder depends on several factors like geometry, Reynolds number and boundary conditions. A lot of work has already been done to study the effect of these parameters on the flow. In the following text, we briefly discuss some literature relating to the effects of these parameters on the flow.

### 1.0.5 Effect of geometry

Several researchers found that the geometry of the cylinder, whether it is square or rectangular or circular, Aspect ratio of the cylinder (for rectangular cylinder, it is defined as the ratio of the height to the width of the cylinder), orientation of the cylinder and position of the cylinder in the domain has significant effect on the flow dynamics. Some of the work from the literature has been discussed here.

Sajjad & Sohn (2014) observed that orientation of a square cylinder has significant effect on shape and size of the recirculation bubble. They observed the effect at four different orientations for a square cylinder,  $\theta = 0, 22.5, 30,$  and  $45$ . They concluded that wake formation and separation processes are asymmetric for angles  $22.5$  and  $30$  degrees. A minimum in drag coefficient and maximum in Strouhal number is observed at a square cylinder orientation of  $22.5$ . The main reason for minimum drag coefficient at  $22.5$  is attributed to the wake asymmetry originating from shear layers of unequal lengths on each side of the cylinder. The wake asymmetry increases the transverse velocity, which further increases the base pressure, and hence lowers

drag. This factor(wake asymmetry) is counterbalanced by an increase in the projected area, but the minimum in the drag coefficient at an orientation of 22.5 reveals that the former has an overall stronger influence at small cylinder angles, and hence the stronger three dimensionality of the flow field at 22.5. Furthermore, they observed that the separation distance between the alternating vortices depend upon the cylinder orientation.

Obasaju (1983) experimentally studied the effect of square cylinder orientation at high Reynolds numbers. The Strouhal number based on the cylinder diameter is found to decrease slightly at first and rise rather abruptly to a maximum when the angle of incidence is 13.5 deg. Reattachment of the shear layer may start at this angle. This effect was attributed to the shear layer reattachment over one of the edges of the cylinder. In 1990, Knisely experimentally investigated the variation of Strouhal number of rectangular cylinders with side ratios in the range of 0.041 and angles of incidence from 0 to 90 degrees. A sharp rise in Strouhal number for a small angle of incidence was reported.

Lee & Budwig (1991) experimentally studied the effect of aspect-ratio for a cylinder at low Reynolds number. They observed that there is a stabilization effect on the wake for a small aspect ratio cylinder (aspect-ratios less than 60) and the wake width increases with a reduction in aspect ratio.

Stäger & Eckelmann (1991) studied the effect of end plates on the shedding frequency of circular cylinders in the intermediate range of Reynolds numbers 300500. They observed that the size of the recirculation bubble is smaller at higher aspect ratio: That is why the drag coefficient is correspondingly smaller. At the lower aspect ratio, the shear layers are stabilized, resulting in higher drag and lower Strouhal number. The stronger three dimensionality of flow at the lower aspect ratio has only a marginal overall effect. They also observed that the turbulence intensity is higher for the larger aspect ratio cylinder since the size of the recirculation bubble is reduced. Correspondingly, the maximum turbulence intensity appears at an earlier streamwise location.

Dipankar *et al.* (2007) studied the effect on vortex shedding of big cylinder when a small cylinder is placed near the wake of big cylinder. They observed drag reduction, decreased shedding frequency and narrowing of wake bubble due to the presence of the small cylinder. Their results matched well with the experimental result of Strykowski & Sreenivasan Strykowski & Sreenivasan (1990)

### 1.0.6 Effect of Boundary conditions

For an unbounded flow, it is very important to choose an optimum domain size so that there should not be any influence of boundaries and should not be computationally expensive as well Behr *et al.* (1995) found that lateral boundaries should be distanced from the cylinder by at least 8 cylinder diameters in order to vanish the effect of lateral boundaries. He also observed that Strouhal number, drag coefficient and lift coefficient increases as lateral boundaries come closer to cylinder.

Sen *et al.* (2009) observed that the blockage (ratio of diameter of the cylinder to the domain width) should be less than 0.01, for the flow to behave as an unbounded flow. The effect of blockage on the Reynolds number at which vortex shedding starts is termed as critical Reynolds number. They observed that critical Reynolds number reduces with increase in blockage initially but up to a certain limit and then decreases with further increase in blockage. They also observed that at critical Reynolds number Strouhal number increases with increase in Blockage.

Muralidhar *et al.* (2011) performed experiments on cylinders with super-hydrophobic surface coating in order to study the effect of surface properties on vortex shedding dynamics. They observed the delay in the onset of vortex shedding and increase in length of recirculation region as compared to uncoated cylinders on which no-slip condition holds. They also observed that even the orientation in which coating is done has lot of significance on vortex shedding dynamics. When the ridges were made to be parallel to the flow direction, an increase in shedding frequency was observed and the separation point was found to move further upstream (towards the front stagnation point of the cylinder) but when the ridges were kept in the perpendicular direction of the flow, the trend reversed i.e. there was a decrease in shedding frequency and separation point moved downstream. They also observed almost 30% reduction in drag as compared to an uncoated cylinders.

Prandtl (1925) was the first one to perform an experiment on rotating cylinder and he concluded that the maximum lift that can be generated by a spinning cylinder in a uniform flow is  $4\pi$ . Later on, Tokumaru & Dimotakis (1993) ? measured experimentally, and they concluded that lift coefficient value can be greater than Prandtl's limit. Much more work has been done on the rotating cylinder. If reader want to go in to detail he/she can refer papers like Mittal & Kumar (2003); Tokumaru & Dimotakis (1993)

### 1.0.7 Effect of oscillations

Bishop & Hassan (1964); Carberry *et al.* (2001); Griffin (1971); Krishnamoorthy *et al.* (2001); Ongoren & Rockwell (1988); Williamson & Roshko (1988) has studied oscillating cylinder in terms of wake region. Detailed mechanism has also been studied by different researchers Bearman (1984); Oertel Jr (1990); Parkinson (1989); Zdravkovich & Carelas (1997). In this subsection some of the work for an oscillating cylinder in the literature, has been discussed.

When a body is oscillating in a uniform flow, different kinds of vortex shedding modes has been observed, symmetric and antisymmetric Carnevale *et al.* (1997). Here, Symmetric mode refer to the mode where the vortices shed from the top are of one sign and vortices shed from the bottom are of another sign, and from both the sides (top and bottom), body will shed simultaneously. Further classification of symmetric mode has been done which is based on the number of vortices shed from each side per cycle. Zhou & Graham (2000) has observed one vortex shed from both the sides(top and bottom), simultaneously. This mode is termed as  $S - I$  mode, where  $S$  denotes symmetry and  $I$  denotes the number of vortices shed per cycle. Konstantinidis & Balabani (2007) observed experimentally  $S - II$  mode, which means two vortices from top and bottom of the cylinder are shed simultaneously which are



of opposite sign (one sign from the top and another from the bottom). Srikanth *et al.* (2011) observed computationally for the first time  $S - II$  mode. Srikanth *et al.* (2011), observed  $S - III$  mode, where they have found two vortices shed from top and bottom of the cylinder and one vortex along the center line of the cylinder.

Leontini *et al.* (2011) studied the inline oscillating cylinder problem, numerically. They showed that the forcing causes the primary shedding frequency to decrease proportionally to the square of the forcing amplitude. As the forcing amplitude is increased, the flow locks-in to a subharmonic of  $f_o$ .

Barbi *et al.* (1986); Griffin & Ramberg (1976); Konstantinidis & Balabani (2007); Konstantinidis *et al.* (2005) studied the synchronization between the forcing and the shedding frequency. They found that the vortex shedding occurs at half the forcing frequency which is termed as "lock-in". This happens particularly, for forcing frequencies  $2f_o$ .

Barbi *et al.* (1986); Ongoren & Rockwell (1988) reported a symmetric wake structure different from the classic von Karman vortex street which typically occurs for high values of forcing frequency. They point out that the occurrence of such shedding pattern depends on the set of amplitude and frequency of forcing used.

Yokoi & Kamemoto (1994) also studied the synchronization between the forcing and shedding frequencies, with an emphasis on the symmetric wake structures as found in Barbi *et al.* (1986); Ongoren & Rockwell (1988). They found several synchronized states as a function of the forcing frequency, amplitude and Reynolds number. These states were found to be synchronized to either the forcing frequency,  $f_e$  or to its first subharmonic i.e.  $f_e/2$ . This phenomenon was noticed for forcing frequency close to the shedding frequency of the corresponding stationary cylinder. This was later confirmed and extended by Cetiner & Rockwell (2001)

Perdikaris *et al.* (2009) numerically investigated the flow past a cylinder oscillating at a frequency equal to the shedding frequency of a stationary cylinder,  $f_o$ , at a Reynolds number of 400. For low forcing amplitudes, the flow behaved similar to that of a stationary cylinder. At high values of amplitudes, they found the shedding to lock-in to the first subharmonic of the forcing. At moderate forcing amplitudes, they found chaos in the wake with irregular vortex shedding. The chaos was attributed to the mode competition between the symmetric forcing and the antisymmetric von Karman vortex street.

Leontini *et al.* (2011) conducted a numerical study at  $Re = 175$ , in order to find the effect of forcing amplitude on a cylinder oscillating with a frequency equal to the shedding frequency of a stationary cylinder. For low to moderate amplitudes, the primary shedding frequency decreased with the increasing amplitude ratio  $a_r = A/D$  as the square of  $a_r$  wherein  $A$  is the amplitude of forcing and  $D$  is the diameter of the cylinder. This was also suggested by Perdikaris *et al.* (2009). The flow dynamics was shown to be governed by the interaction of the shedding frequency and the forcing frequency which resulted in a frequency and amplitude modulated flow. However, the behaviour was found to be non-linear when the forcing frequency became a multiple of the primary shedding frequency. In this scenario, a series of subharmonics were discovered ranging from the 1/8th mode at low amplitudes to the 1/2 subharmonic at higher amplitudes.

Tudball-Smith *et al.* (2012) investigated the effect of forcing amplitude on the shedding frequency of cylinders. The forcing frequency  $f_e$ , for most part of the study, has been kept equal to the shedding frequency of the stationary cylinder ( $f_o$ ). They found the similar behaviour when the shape of the cylinder was changed from circular to a square one. They also reported that the dynamics reported in previous studies Perdikaris *et al.* (2009) Leontini *et al.* (2011) persists even at higher Reynolds numbers. Thus, the authors concluded that the physical mechanism is applicable to the periodic forcing of the von Karman vortex street, regardless of the body features.

Khaledi *et al.* (2012) studied flow past an inline oscillating normal flat plate to investigate the various wake phenomena at a low Reynolds number ( $= 100$ ). They found that at low excitation frequencies, the wake vortex shedding is antisymmetric. When the forcing frequency is increased, the wake becomes chaotic and then turns into symmetric mode. On increasing the forcing frequency further, a more complex symmetric wake pattern was observed before, ultimately, it turned into chaos. In a particular case, the S-II mode in the near wake, turned into a new S-IV mode, comprising of four different vortex pairs per shedding cycle.

Xu *et al.* (2006) experimentally studied the flow past inline oscillating cylinder. They reported a new symmetrical vortex shedding mode at higher frequency ratios after Ongoren & Rockwell (1988) reported their first symmetrical mode. In their theoretical analysis, they predicted the onset of the S-II mode. They argued that the binary vortex formed by two counter-rotating vortices can only be produced when the cylinder moves against the incoming flow direction and showed that the S-II mode arises when the relative Reynolds number  $Re = \rho(2\pi f_e A - U_{in})D/\mu$  exceeds a critical value. This critical value is related to a critical value of the excitation frequency which varies inversely with the amplitude ratio  $a_r = A/D$ .

Dutta *et al.* (2007) experimentally investigated the effect of excitation frequency and amplitude on the vortex shedding. They found that an increase in the forcing frequency led to a substantial reduction in the recirculation length and the time-averaged drag coefficient. Similarly, they showed that by increasing the forcing amplitude, the time-averaged drag coefficient and the recirculation length decreased while the peak rms velocity increased.

Srikanth *et al.* (2011) studied the flow past inline oscillating cylinders at  $Re = 200$ . They performed lattice-Boltzmann simulations to explore the different modes of shedding in the wake of a rectangular cylinder for various aspect ratios. They also investigated the competition between the symmetric and anti-symmetric modes which leads to chaos. For a particular amplitude and frequency ratio combination, the authors were able to find a new S-III vortex shedding mode.

### 1.0.8 Structure of the thesis

We have briefly discuss about the introduction, literature survey and motivation of the problem in this section. In the next section, i.e. chapter2 of the thesis we have discuss about the numerical formulation, in chapter 3 we have discuss about results and has given concluding remarks

in chapter 4.



# CHAPTER 2

## Formulation

In this thesis we study flow past an oscillating (in a stream-wise direction) rectangular body, in a uniform flow. To simplify the computational study, we model this problem by considering a stationary rectangular body in an oscillating flow (imposed at the inlet), and we have neglected the added mass effect. Added mass or virtual mass is the inertia added to a system because an accelerating or decelerating body must move (or deflect) some volume of surrounding fluid as it moves through it. For simplicity this can be modeled as some volume of fluid moving with the object, though in reality "all" the fluid will be accelerated, to various degrees. We have neglected it to reduce the complexity of the problem so that the Navier-Stokes and the continuity equations will remain same for the cylinder-fixed frame and the lab frame in the absence of cylinder oscillations. In figure 2.1, left panel shows the actual problem, and right side panel shows the simplified computational model .

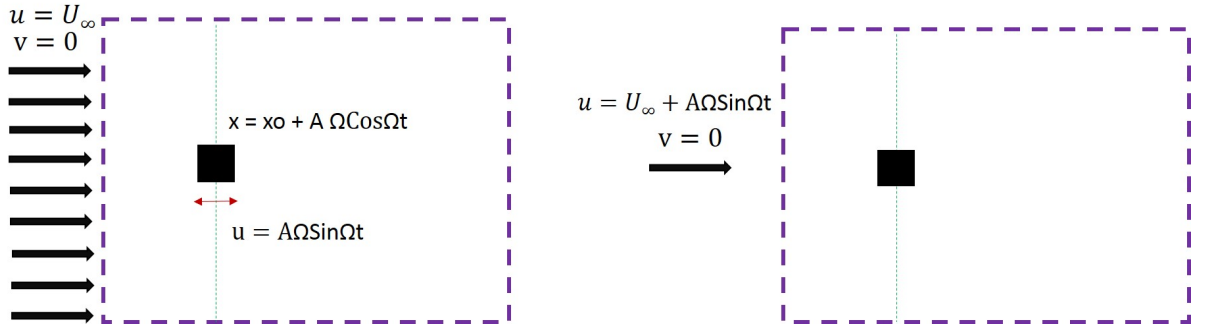


**Figure 2.1:** Schematic showing the actual problem (which we want to study) and the analogous problem (which we have modeled)

A rectangular coordinate system  $(x, y)$  is used to model the flow dynamics, where  $x$  and  $y$  denote the coordinates in the horizontal and vertical directions, respectively. We have considered a rectangular body, which is kept in a domain size of  $200 \times 200$  at a distance of 22 units from the inlet in the  $x$  direction. We have taken a large domain size to ensure that the wake region is insensitive to the lateral and longitudinal boundary conditions. A Newtonian fluid of viscosity  $\mu$  and density  $\rho$  is injected from the inlet. We have considered an oscillating inlet flow,  $u = U_\infty + A \omega \sin(\omega t)$  where,  $A$  is the amplitude of the displacement of the body,  $\omega = 2\pi f_e$  is the frequency of the oscillation,  $u$  is the stream-wise velocity of fluid and  $v$  is the transverse fluid velocity, as shown in Fig. 2.2. We have imposed no-slip condition, i.e.  $u = 0$  and  $v = 0$  at the surface of cylinder, and neumann boundary condition at the outlet of the domain. The top and bottom of the domain has symmetry boundary condition. We have used nonuniform grids of up to a million grid points, as in Fig. 2.3.

Same boundary conditions at the top and bottom as inlet

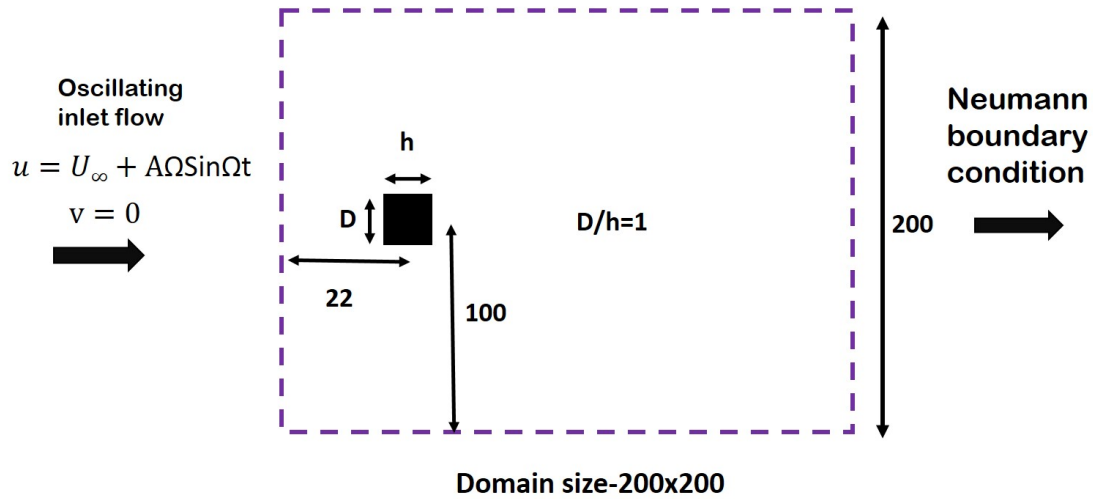


**Figure 2.2:** Schematic showing the geometry (not to scale) with an oscillating inlet at  $x = 0$ .

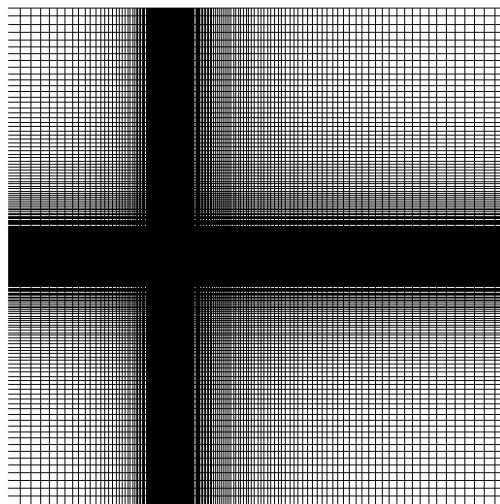


**Figure 2.3:** Schematic showing the non-uniform grid.

## 2.1 Numerical method

We have used two numerical methods, lattice Boltzmann method and open source code, gerris. First we have discussed lattice Boltzmann method and then briefly about gerris.

### 2.1.1 Introduction to lattice Boltzmann method

The LBM is an alternative computational method to simulate fluid flows. It is a mesoscopic model that has its origin in the kinetic theory and is derived from lattice gas automata. The LBM solves discrete density distribution functions and obtains the velocities and densities as moments of this distribution function. Starting with the lattice Boltzmann equation, one can obtain Navier-Stokes equations, as shown in appendix. In comparison with Navier-Stokes equations. LBM is simple, efficient and easily parallelizable technique. The explicit nature of this method and the absence of the pressure poisson equation which is the most time consuming step in others methods, make this method computationally very economical. It has only three steps:

- (1) collision;
- (2) streaming; and
- (3) calculation of the variables.

Streaming and collision are the successive steps. In streaming, the distribution functions get updated according to the discrete velocity direction which has been assigned in the collision step as per the collision rule. Distribution functions get updated for each lattice at every time step, taking care of the fact that it should follow mass and momentum conservation, as shown in Fig. 2.4. Once all the distribution functions are updated at all the nodes, one can calculate macroscopic variables like pressure, velocity and density.

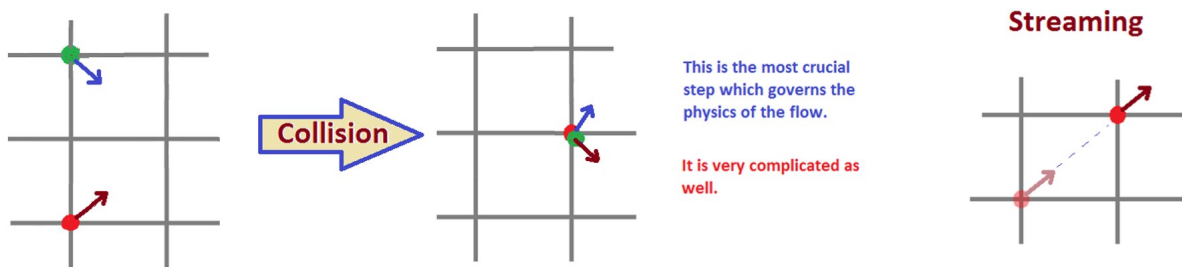


**Figure 2.4:** Schematic streaming and collision at each time step.

The single-phase lattice Boltzmann method used in the present study is similar to an earlier study of Dixit & Babu (2006). According to kinetic theory, single particle density distribution obeys Boltzmann equation.

$$(\partial_t + v \cdot \nabla)f = \Omega(f) \quad (2.1)$$

In 2.1  $f$  is the single particle density distribution function,  $v$  is the microscopic velocity and  $\Omega$  is the collision term.

Considering the effect of the external forces and using BGK approximation, equation 2.1 will become

$$(\partial_t + v \cdot \nabla)f = -\frac{f - f_{eq}}{\tau_v} \quad (2.2)$$

In equation 2.2,  $\tau_v$  is the relaxation time using the Bhatnagar-Gross-Krook (BGK) model [Bhatnagar *et al.* (1954)],  $f_{eq}$  is the Maxwell-Boltzmann equilibrium distribution function given by

$$f^{eq} = \frac{\rho}{(2\pi RT)} \exp \frac{-(v - u)^2}{2RT}, \quad (2.3)$$

### 2.1.2 D2Q9 model

In LBM, we have to choose a discretized velocity model as per our requirement. In literature, the lattice models are commonly designated as  $DxQy$  model, where  $x$  denotes the space dimension and  $y$  denotes the number of possible velocity direction.  $D2Q7$ ,  $D2Q9$ ,  $D3Q15$ ,  $D3Q19$  and  $D3Q27$  are some commonly used models available in the literature. The lattice model restricts the fluid molecules to move in certain specified directions. At each time, the distribution function is advected to its nearest neighbour along a direction specified by the collision rules. If two distribution functions arrive at the same point, then they are redistributed as per the collision rules, so as to conserve mass and momentum. The speed of sound in the lattice and the weights in the equilibrium distribution functions are the lattice dependent quantities.

In this present simulation, the evolution equations are simulated with a two-dimensional nine-velocity model ( $D2Q9$ ), as shown in figure 2.5, where

$$v_i = \begin{cases} 0, & i = 0 \\ \left[ \cos\left(\frac{(i-1)\pi}{2}\right), \sin\left(\frac{(i-1)\pi}{2}\right) \right], & i = 1, 2, 3, 4 \\ \sqrt{2} \left[ \cos\left(\frac{(i-5)\pi}{2} + \frac{\pi}{4}\right), \sin\left(\frac{(i-5)\pi}{2} + \frac{\pi}{4}\right) \right], & i = 5, 6, 7, 8. \end{cases} \quad (2.4)$$

The weighing coefficients,  $w_i$  are given by:

$$w_i = \begin{cases} 4/9, & i = 0 \\ 1/9, & i = 1, 2, 3, 4 \\ 1/36, & i = 5, 6, 7, 8. \end{cases} \quad (2.5)$$

Here  $i$  is the position of the node in the lattice.

After discretization of 2.2, we have:



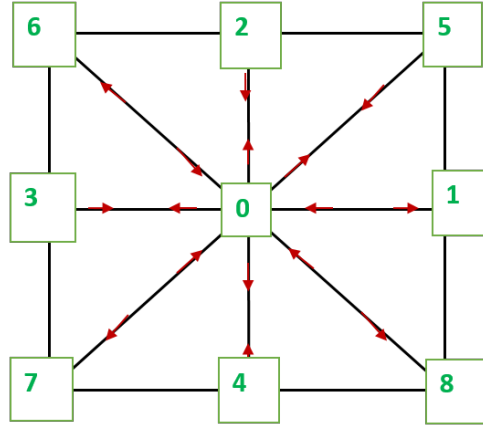


Figure 2.5: D2Q9 model

$$f_i(\mathbf{x} + \mathbf{v}_i \delta t, t + \delta t) - f_i(\mathbf{x}, t) = -\frac{f_i(\mathbf{x}, t) - f_i^{\text{eq}}(\mathbf{x}, t)}{\tau_v}, \quad (2.6)$$

Where, equilibrium function for the density distribution function is given as

$$(f_i)^{\text{eq}} = \mathbf{w}_i \rho \left[ 1 + \frac{\mathbf{v}_i \cdot \mathbf{u}}{c_s^2} + \frac{(\mathbf{v}_i \cdot \mathbf{u})^2}{2c_s^4} - \frac{\mathbf{u}^2}{2c_s^2} \right]. \quad (2.7)$$

Here,  $\mathbf{w}_i$  is the weight function according to the distance of the node from the master node of the lattice. The kinematic viscosity,  $\nu$  is related to the relaxation time as  $\nu = (\tau_v - 1/2)\delta t c_s^2$ , where  $c_s^2 = 1/3$ .

### 2.1.3 Calculation of variables

Macroscopic variables like density, velocity and pressure are calculated as:

$$\rho = \sum f_i \quad (2.8)$$

$$\rho \mathbf{u} = \sum f_i \mathbf{v} \quad (2.9)$$

$$p = \rho (c_s)^2 \quad (2.10)$$

### 2.1.4 Boundary conditions

In LBM, we need to implement the boundary conditions in terms of the distribution function. The boundary conditions for the distribution function should be such that it resembles the desired macroscopic boundary conditions. While it is easier to find the macroscopic flow variables from the distribution functions, the reverse is not so easy. The bounce-back scheme is the simplest and widely accepted model for no-slip boundary condition. It is inspired from LGCA and is easy to implement. However, it is of first order in numerical accuracy. Since the LBE governing equations are second order accurate, the bounce-back scheme degrades the solution near the boundaries. Given the simplicity of the bounce-back boundary conditions and the fine grid (as a result of grid stretching) that we have used in our simulations, the solutions can be expected to be acceptable within the tolerance equivalent to the smallest grid size value. In this scheme, the distribution function of the imaginary nodes outside the domain are updated with the spatially opposite node's distribution function. It is similar to the symmetry boundary condition used for primitive variables in a Navier-Stokes solver. This scheme conserves the mass, whereas momentum is not conserved, which may introduce errors in the solution. This scheme assures that the time-average of the discrete velocities (9 for D2Q9 model) vanishes at the boundary. Specifically, the boundary conditions are implemented as follows.

Free slip boundary condition is imposed on the top and bottom boundaries of the domain. Thus, at the top face, the distribution functions are calculated as:

$$f_4(i, ny) = f_2(i, ny), \quad (2.11)$$

$$f_7(i, ny) = f_6(i, ny), \quad (2.12)$$

$$f_8(i, ny) = f_5(i, ny), \quad (2.13)$$

$$(2.14)$$

Similarly, at the bottom boundary,

$$f_2(i, ny) = f_4(i, ny), \quad (2.15)$$

$$f_5(i, ny) = f_8(i, ny), \quad (2.16)$$

$$f_6(i, ny) = f_7(i, ny), \quad (2.17)$$

$$(2.18)$$

At the inlet and outlet, the distribution function is assumed to take its equilibrium value i.e.  $f_i = f_i^{eq}$ . The boundary conditions for the density at the inlet and outlet is implemented as follows:

$$\rho_{1,j} = \rho_\infty; \quad \rho_{nx,j} = \rho_{nx-1,j}, \quad (2.19)$$

## 2.2 Dimensionless numbers

The various dimensionless parameters describing the flow characteristics are as follows:

- a) Reynolds number,  $Re(\equiv \rho U_\infty D / \mu)$
- b) Frequency ratio,  $f_r(\equiv f_e / f_s)$
- c) Amplitude ratio,  $a_r(\equiv A / D)$
- d) Aspect ratio,  $AR(\equiv D / H)$

Here,  $\rho$  is the density of the flowing fluid,  $\mu$  is the dynamic viscosity,  $f_e$  is the frequency of oscillation,  $f_s$  is the natural vortex shedding frequency (for a non oscillatory case),  $D$  is the height of the cylinder,  $U_\infty$  is the velocity for non oscillatory case,  $A$  is the amplitude of oscillation,  $H$  is the width of the cylinder.

$Re$  has been fixed a value of 200.

$AR$  has been fixed a value of 4 or 1.

$f_r$  and  $a_r$  has been varied.

Strouhal number,  $St(\equiv (f_s D) / U_\infty)$

is an output parameter for a non-oscillatory case. We have measured it and compared it with the literature which shows an agreement with the paper by Okajima (1982).

The domain and grid independency tests would be shown in the results section.



# CHAPTER 3

## Results and discussion

As discussed in the chapter 2 of thesis , we have considered a domain size of  $200 \times 200$  in which cylinder is kept at a distance of 22 units from the oscillatory inlet in the positive  $x$  direction. In this chapter we have discussed all the results which has been obtained from the above described geometry using numerical approach: lattice Boltzmann method . In chapter 2, figure 2.1 we have imposed inlet boundary condition for the velocity as  $u = U_\infty + A\omega\sin(\omega t)$ . If  $U_\infty > A\omega$  then  $u > 0$  for all time. If  $U_\infty < A\omega$  , then it is a part of reverse flow which we are not considering. We have confined our study to the particular region as shown in 3.1, where there is no reverse flow. In 3.1,  $Y$  axis represent frequency ratio and  $X$  axis represents the amplitude ratio. The hyperbolic curve shown in 3.1 is the upper limit of our study where  $U_\infty = A\omega$  i.e. we are interested in the region below this curve where there is no reverse flow. Above this curve, reverse flow will occur, which we have not investigate. As discussed in chapter 1 we expect symmetric mode in the vicinity of the hyperbola boundary .

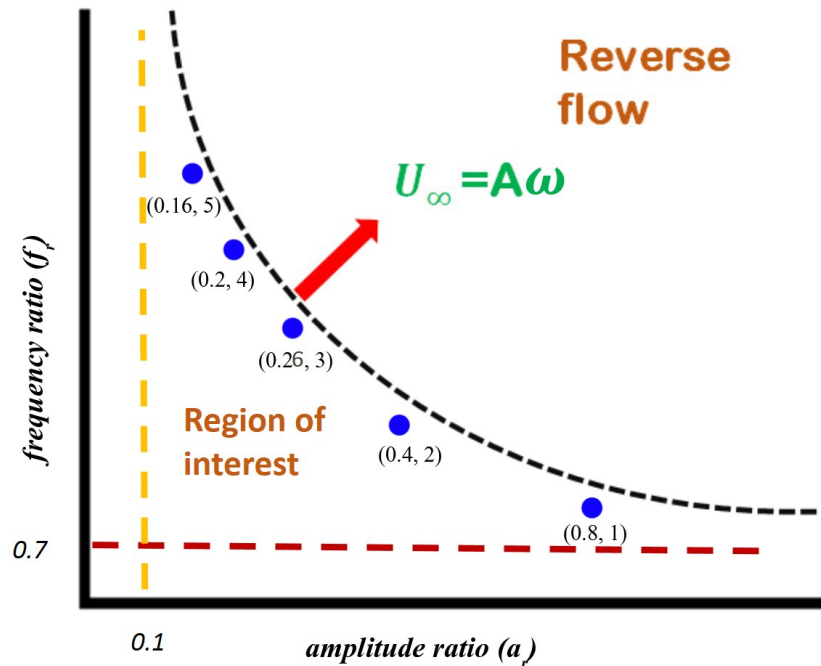


**Figure 3.1:** Schematic showing the region of interest for the defined problem, with no reverse flow (not to scale).

## 3.1 Results obtained from lattice Boltzmann method

### 3.1.1 Grid Independence Test

We begin presenting our results by conducting a grid convergence test for a square body. In Fig. 3.2 (a), (b) and (c), the contours of the vorticity are shown, for  $Re = 100$ , for a frequency ratio  $f_r = 2$  and for an amplitude ratio  $a_r = 0.5$ . The flow dynamics obtained using the different grids look qualitatively similar.

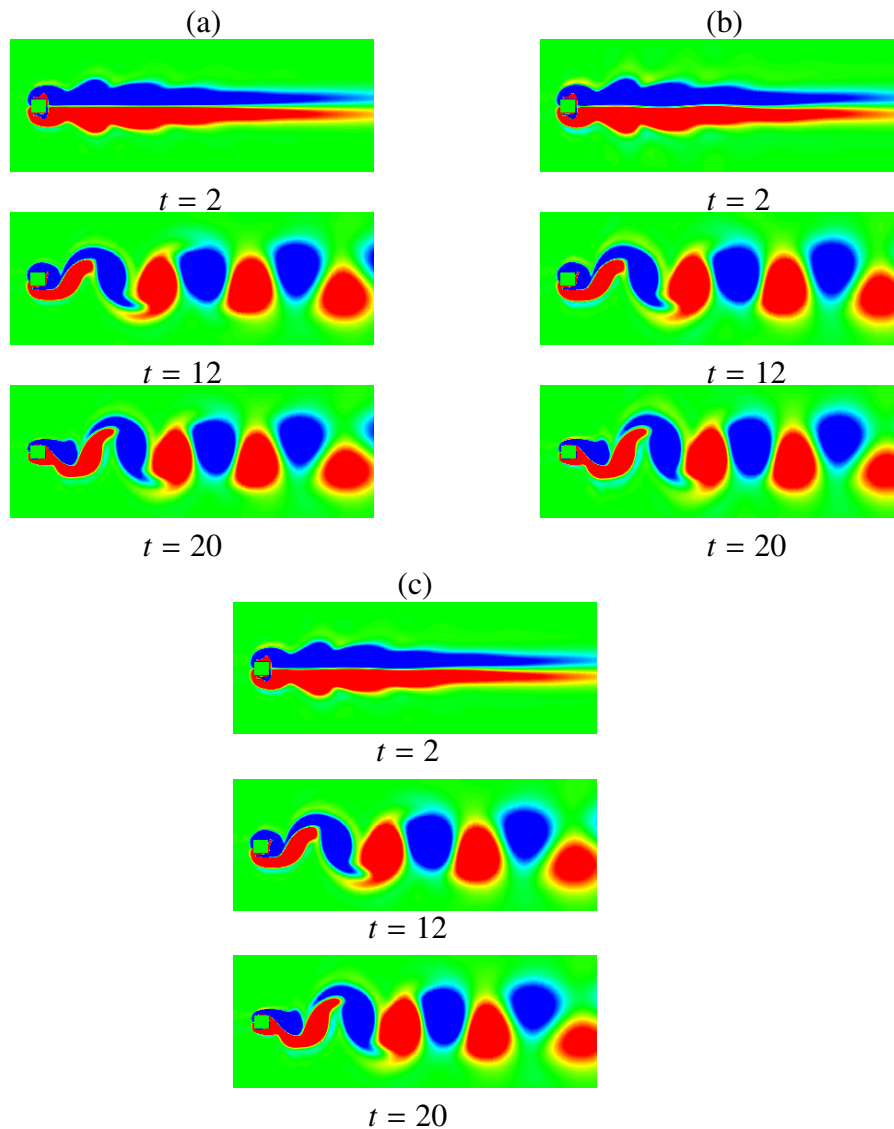


**Figure 3.2:** Contours of the vorticity for a square cylinder, (a) 80 points per unit length on the body surface, (b) 120 points per unit length on the body surface, (c) 160 points per unit length on the body surface. The rest of the parameters are  $Re = 100$ ,  $f_r = 2$ ,  $a_r = 0.5$ .

### 3.1.2 Domain independence test

As discussed previously, we are considering an unbounded flow. We have carried out domain independence test in order to verify that flow does not have any effect of lateral as well as longitudinal boundaries. We have considered three domain sizes  $300 \times 300$ ,  $400 \times 400$ , and  $500 \times 500$ . In 3.3 contours of vorticity are shown for domain size a)  $300 \times 300$  b)  $400 \times 400$  c)  $500 \times 500$  at different  $t$  are shown which look similar. Thus domain independence test has been achieved.

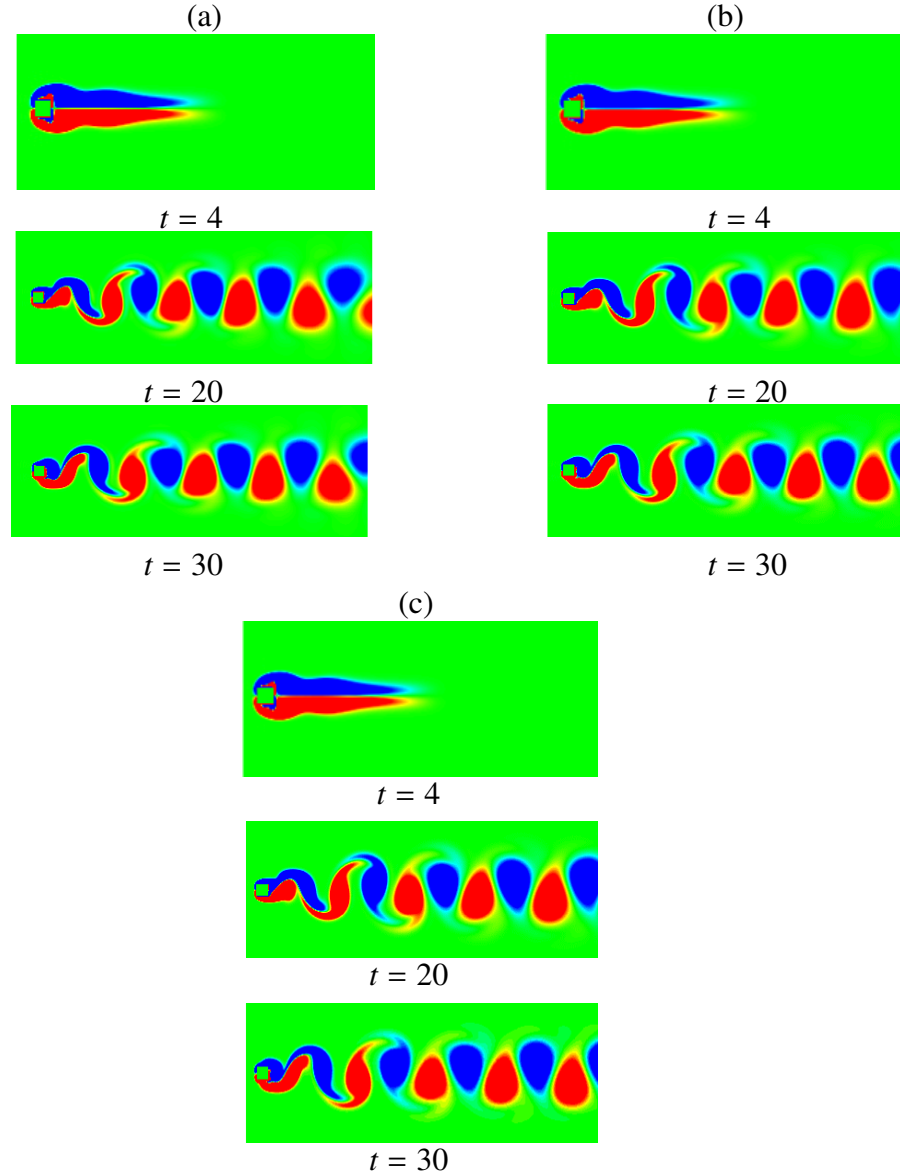


**Figure 3.3:** Contours of the vorticity, (a)  $300 \times 300$ , (b)  $400 \times 400$ , (c)  $500 \times 500$ . The rest of the parameters are  $Re = 100$ ,  $f_r = 2$ ,  $a_r = 0.5$ .

### 3.1.3 Comparison with the literature

In 3.4, the left hand side graph shows the power spectrum, in which  $Y$  represents the power and  $X$  axis represents the non-dimensional frequency. We have calculated the strouhal number,  $St$  from the spectrum obtained for a square cylinder. A prominent peak in the power spectrum is obtained at  $f = 1.71 \times 10^{-4}$ , which corresponds to a strouhal number,  $St = f_s D / U_\infty = 0.137$ . The right hand side picture of 3.4 is taken from the Okajima (1982) literature which represent strouhal number,  $st$  on  $Y$  axis and Reynolds number,  $Re$  on the  $X$  axis. The strouhal number  $st$  obtained from the power spectrum using LBM code matches well with Okajima (1982).

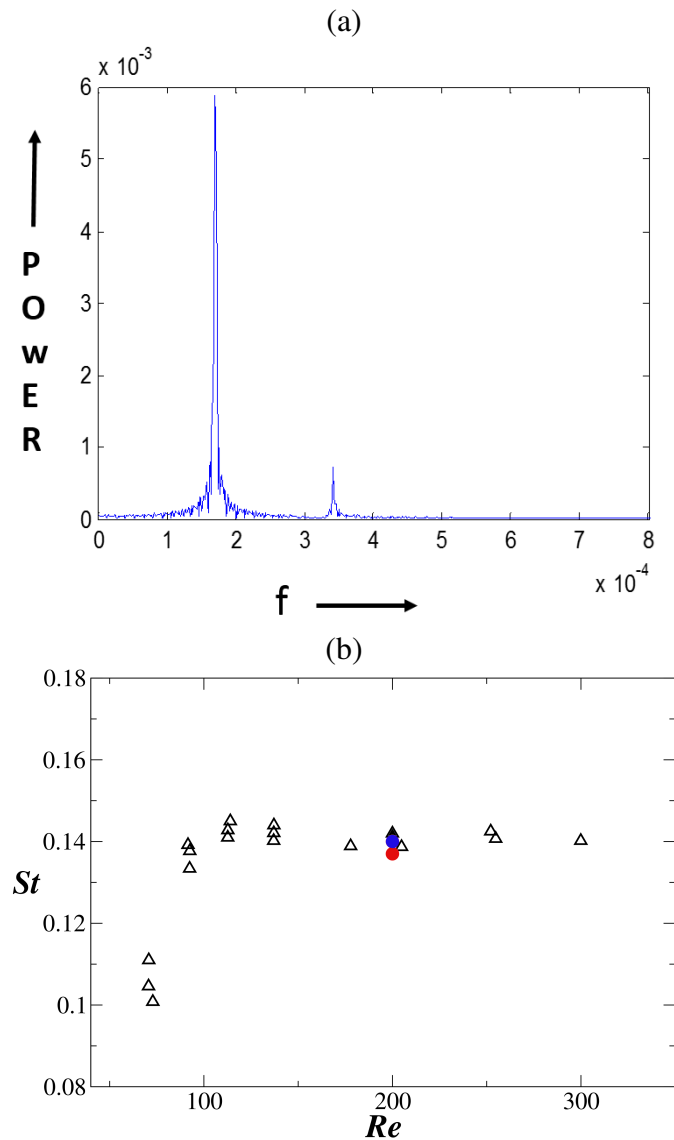


**Figure 3.4:** (a) Graph showing the power spectrum obtained from the code for the calculation of Strouhal number,  $St$  for the non-oscillating square cylinder and (b) variation of Strouhal number,  $st$  with Reynolds number,  $Re$  as found by Okajima (1982). Shown in the red are the Strouhal number obtained from our code and in blue dot from gerris.



### 3.1.4 Antisymmetric to symmetric mode

We have considered the cases for the values of  $f_r$  and  $a_r$  along the three lines as shown in figure 3.1:

- (a) Keeping  $f_r$  fixed and varying  $a_r$ , shown by red color dotted line.
- (b) Keeping  $a_r$  fixed and varying  $f_r$ , shown by yellow color dotted line.
- (c) Varying both  $a_r$  and  $f_r$  along the hyperbolic curve, as shown by blue dots.

In the following subsection, we have shown the results for the above mentioned cases.

#### 3.1.5 (a) Varying amplitude ratio

In 3.5 shows conversion from antisymmetric vortex shedding mode to symmetric mode for a square cylinder, at a frequency ratio,  $f_r$  of 0.7 for different amplitude ratio's a)  $a_r = 0.1$  b)  $a_r = 0.5$  c)  $a_r = 1.1$  d)  $a_r = 1.65$ . In figure 3.5 (a) where,  $a_r = 0.1$  we have an antisymmetric pattern, with a vortex being shed from top and bottom alternately. In figure 3.5 (b), we obtain a mixed mode,  $a_r = 0.5$ . In this mode, vortex is being shed in an alternating way but in an oscillatory manner i.e. in this mode one more frequency is added to the previous [(a)] mode which is making it oscillatory. In figure 3.5 (c),  $a_r = 1.1$  we obtain a chaotic mode which means vortex is being shed with multiple frequencies and there is no repetition in the pattern. In figure 3.5 (d), at  $a_r = 1.65$  we have obtained a symmetric mode of vortex shedding in which initially two vortex of different sign are shed simultaneously from top and bottom of the cylinder which are then merging to form single vortex at the top and bottom. This mode is called as  $S - 21$  mode. To the best of my knowledge this mode has never been reported before in the literature. In figure 3.5 right hand side corresponds to phase plots. The  $Y$ , axis on the phase plots represent  $v(t + \tau)$  and  $X$ , axis represent  $v(t - \tau)$  at a suitably chosen location and delay time,  $\tau$ . In figure (a) and (d) 3.5, the paths in phase plots are closed bands which shows periodicity where as in (c) part phase plot is completely filled which represent chaos.

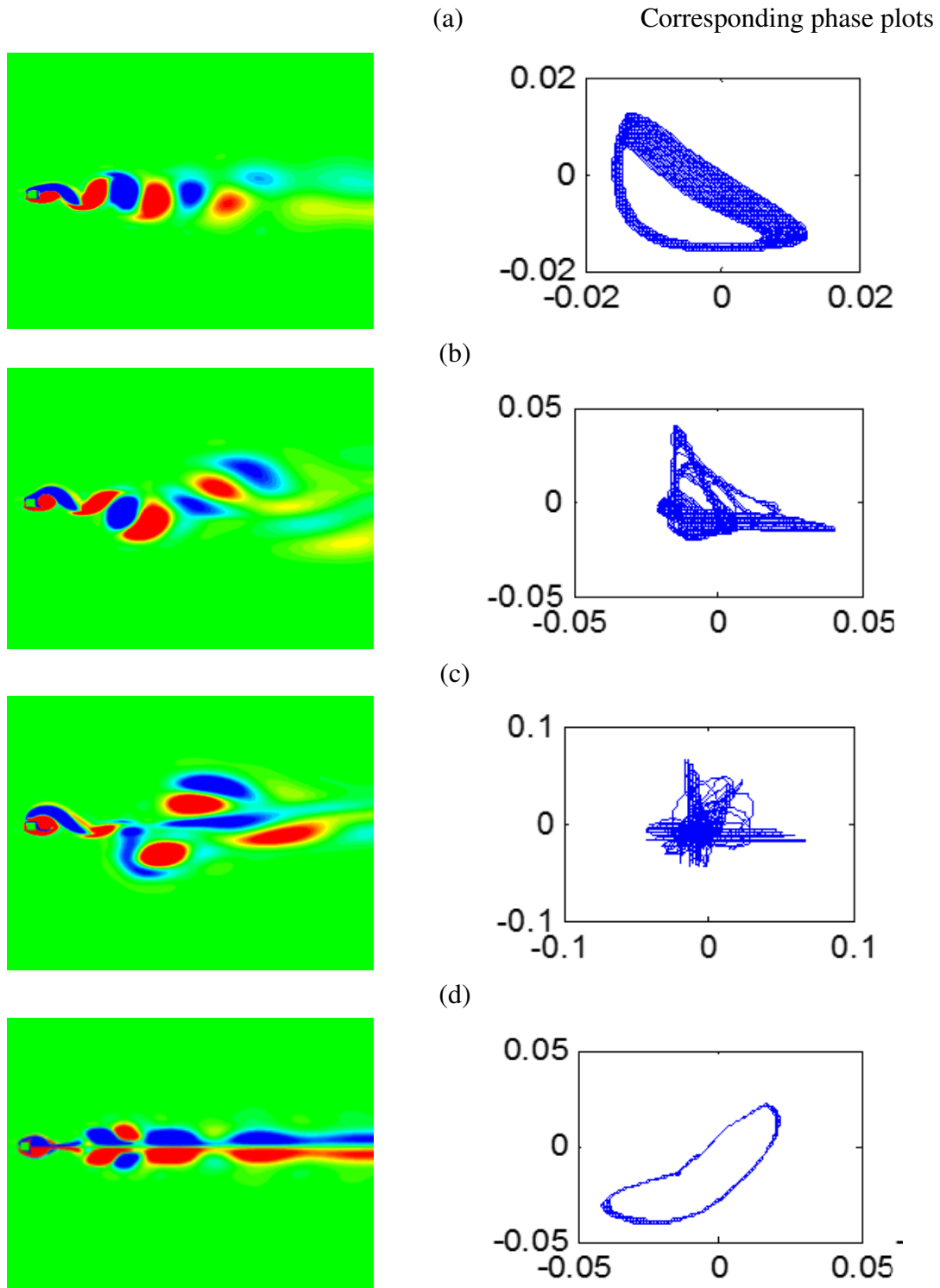


**Figure 3.5:** Schematic showing the contours of the vorticity for a square cylinder, which is showing different vortex shedding pattern with phase plots at different points in the domain. The parameters are Reynolds number,  $Re = 100$ , frequency ratio,  $f_r = 0.7$ , amplitude ratio: a)  $a_r = 0.1$  b)  $a_r = 0.5$ , c)  $a_r = 1.1$ , d)  $a_r = 1.65$ .

### 3.1.6 (b)Varying frequency ratio

In this part we have shown the vortex shedding modes going along the yellow line in figure 3.1. We have observed that keeping the amplitude ratio,  $a_r$  fixed and varying the  $f_r$  does not have much difference on vortex shedding modes. As shown in figure 3.6 we have obtained antisymmetric mode of vortex shedding for all  $f_r$  keeping the  $a_r$  fixed.

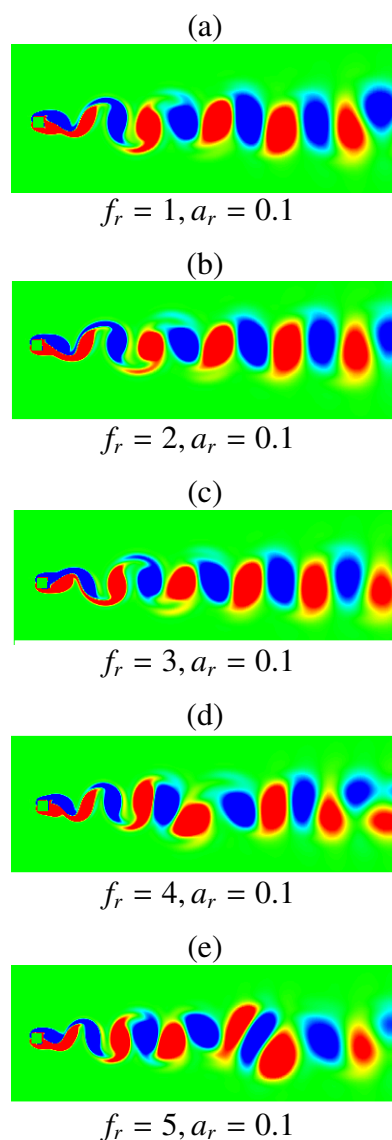


**Figure 3.6:** Schematic showing the contours of vorticity for a square cylinder along the yellow dotted line, as shown in figure 3.1 . The parameters are Reynolds number,  $Re = 100$  The values for frequency and amplitude ratio's are: a)  $f_r = 1, a_r = 0.1$  b)  $f_r = 2, a_r = 0.1$ , c)  $f_r = 3, a_r = 0.1$ , d)  $f_r = 4, a_r = 0.1$ ,  $f_r = 5, a_r = 0.1$  .

### 3.1.7 Varying frequency ratio and amplitude ratio simultaneously

Based on the paper by Srikanth *et al.* (2011), we expect symmetric modes of shedding in the border shown in 3.1 but with the LBM code we have not achieved what we had expected. 3.7 shows the results which we had for the border shown in 3.1 .In 3.1 1 corresponds to  $f_r = 1, a_r =$ , 2 corresponds to  $f_r = 2, a_r =$ , 3 corresponds to  $f_r = 3, a_r =$ , 4 corresponds to  $f_r = 4, a_r =$ , 5 corresponds to  $f_r = 5, a_r =$  Moreover, LBM code has not given correct solution for very low amplitude ratio  $a_r = 0.005$ , for a very long time period.

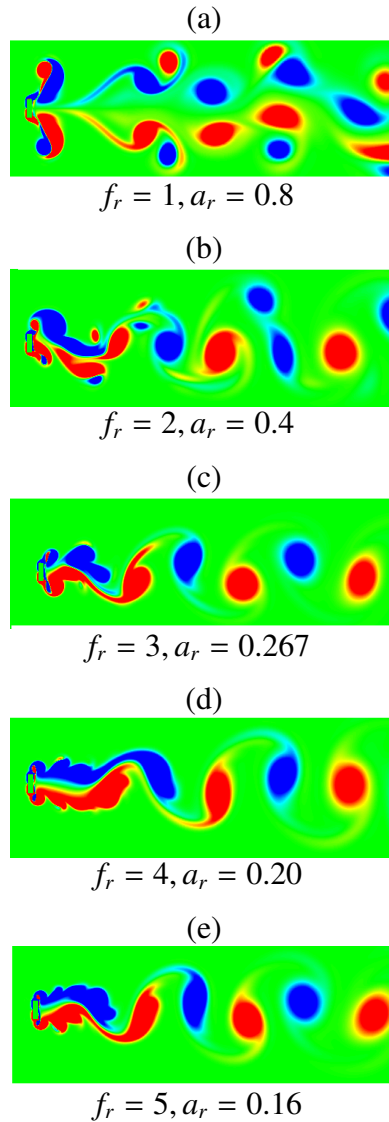


**Figure 3.7:** Schematic showing the contours of vorticity, for a rectangular cylinder for the borderline cases as shown in figure 3.1 . The parameters are Reynolds number,  $Re = 200$  The values for frequency and amplitude ratio's are: a)  $f_r = 1, a_r = 0.8$  b)  $f_r = 2, a_r = 0.4$ , c)  $f_r = 3, a_r = 0.26$ , d)  $f_r = 4, a_r = 0.2$ ,  $f_r = 5, a_r = 0.16$  .

# CHAPTER 4

## Concluding remarks

In this thesis, an oscillatory flow over a rectangular cylinder has been investigated by varying the amplitude and frequency of the imposed flow. The region without reverse flow at the inlet of the computational domain is only considered. The objective of this thesis is to understand the formation of different vortex shedding modes and the transition from one mode to another as the frequency and amplitude ratio are varied. This is an industrially relevant problem commonly found in many industrial processes, such as structural designing, aerodynamics, wind engineering, electronics cooling, etc. A lattice Boltzmann method is used in order to simulate this problem with non-uniform meshes. It is well known that LBM gives higher computational efficiency over the standard Navier-Stokes solvers, as all the steps in LBM are explicit in nature. The pressure-Poisson equation, which is the most time consuming part in any Navier-Stokes solvers, is not present in LBM approach. This is the main reason of the increasing popularity of this method.

The problem considered in the thesis is an extremely difficult problem computationally as in order to get any accurate solution one has to use very fine mesh near the cylinder. In order to overcome this difficulty, a non-uniform mesh has been used in the present LBM solver.

As discussed in Chapter 2, a periodically oscillatory flow is imposed at the beginning of the computational domain. The rectangular cylinder is placed slightly away from the inlet. In order to obtain results, which are independent from the size of the computational domain and grid used, a very large computational domain is considered and a grid convergence has been conducted.

The results presented in Chapter 3 show that for higher amplitude ratio symmetric vortex shedding is observed. For frequency ratio 0.7, it is found that for lower amplitude ratio the vortex-shedding pattern is antisymmetrical; for intermediate amplitude ratio chaotic mode is observed and symmetric shedding is found for higher amplitude ratio. For a fixed amplitude ratio 0.1, and varying the frequency ratio, we have not observed much difference in vortex shedding mode. Thus for getting different vortex shedding mode, one has to vary amplitude ratio's. Hence probability of getting symmetric modes is for low frequency ratio and for a high range of amplitude ratio. In future, I plan to conduct a more comprehensive study on this subject and will explore the relevant physics in details.



# APPENDIX I

## Navier-Stokes equation from the Boltzmann equation

Maxwell-Boltzmann equilibrium distribution function is given by

$$f^0(\mathbf{v}) = \frac{n}{(2\pi\theta)^{3/2}} e^{-[(\mathbf{v}-\mathbf{u})^2/2\theta]}. \quad (\text{I.1})$$

In this section we are showing the proof of the following important identities which will be used in the subsequent derivations.

$$\int_{-\infty}^{\infty} f^0 = n, \quad (\text{I.2})$$

$$\int_{-\infty}^{\infty} f^0(v_i - u_i) = 0, \quad (\text{I.3})$$

$$\int_{-\infty}^{\infty} f^0(v_i - u_i)(v_j - u_j) = n\theta\delta_{ij}, \quad (\text{I.4})$$

$$\int_{-\infty}^{\infty} f^0(v_i - u_i)(v_j - u_j)(v_\gamma - u_\gamma) = 0, \quad (\text{I.5})$$

$$\int_{-\infty}^{\infty} f^0(v_i - u_i)(v_j - u_j)(\mathbf{v} - \mathbf{u})^2 = 5n\theta^2\delta_{ij}. \quad (\text{I.6})$$

### .1 Proof of Eq. (I.2)

Left hand side of Eq. (I.2) is given by

$$\begin{aligned} \int_{-\infty}^{\infty} f^0 d\mathbf{v} &= \int_{-\infty}^{\infty} \frac{n}{(2\pi\theta)^{3/2}} e^{-(\mathbf{v}-\mathbf{u})^2/2\theta} d\mathbf{v} \\ &= \frac{n}{(2\pi\theta)^{3/2}} \int_{-\infty}^{\infty} e^{-(v_1-u_1)^2/2\theta} dv_1 \int_{-\infty}^{\infty} e^{-(v_2-u_2)^2/2\theta} dv_2 \int_{-\infty}^{\infty} e^{-(v_3-u_3)^2/2\theta} dv_3 \\ &= \frac{n}{(2\pi\theta)^{3/2}} I^3, \end{aligned} \quad (\text{I.7})$$

where

$$I = \int_{-\infty}^{\infty} e^{-(v_1 - u_1)^2 / 2\theta} dv_1.$$

Let  $t = v_1 - u_1 \implies dt = dv_1$

So,

$$I = \int_{-\infty}^{\infty} e^{-t^2 / 2\theta} dt = \sqrt{2\pi\theta}.$$

So, Eq. (I.7) can be written as

$$\begin{aligned} \int_{-\infty}^{\infty} f^0 dv &= \frac{n}{(2\pi\theta)^{3/2}} I^3 \\ &= \frac{n}{(2\pi\theta)^{3/2}} ((2\pi\theta)^{1/2})^3 \\ &= n. \end{aligned}$$

## .2 Proof of Eq. (I.3)

Left hand side of Eq. (I.3) is given by

$$\begin{aligned} \int_{-\infty}^{\infty} f^0(v_i - u_i) dv &= \int_{-\infty}^{\infty} \frac{n}{(2\pi\theta)^{3/2}} e^{-(v-u)^2 / 2\theta} (v_i - u_i) dv \\ &= \frac{n}{(2\pi\theta)^{3/2}} \int_{-\infty}^{\infty} e^{-(v_1 - u_1)^2 / 2\theta} (v_i - u_i) dv_1 \int_{-\infty}^{\infty} e^{-(v_2 - u_2)^2 / 2\theta} dv_2 \int_{-\infty}^{\infty} e^{-\frac{(v_3 - u_3)^2}{2\theta}} dv_3 \\ &= \frac{n}{(2\pi\theta)^{3/2}} I_1 \times I_2 \times I_3, \end{aligned}$$

where  $i$  can take values 1, 2, 3.

For  $i = 1$ ,

$$I_1 = \int_{-\infty}^{\infty} e^{-(v_1 - u_1)^2 / 2\theta} (v_1 - u_1) dv_1.$$

Let  $t = (v_1 - u_1)^2 \implies dt = 2(v_1 - u_1) dv_1$

So,

$$I_1 = \int_{-\infty}^{\infty} e^{-t/2\theta} dt = 0.$$

Similarly, for  $i = 2$ , it can be shown that  $I_2 = 0$  (keeping ' $v_2 - u_2$ ' in  $I_2$  term).

and for  $i = 3$  it can be shown that  $I_3 = 0$  (keeping ' $v_3 - u_3$ ' in  $I_3$  term).

So, for any values of  $i$  we have,  $I_1 \times I_2 \times I_3 = 0$ .

So, LHS :

$$\int_{-\infty}^{\infty} f^0(v_i - u_i) dv = \frac{n}{(2\pi\theta)^{3/2}} \times 0 = 0.$$



### .3 Proof of Eq. (I.4)

Left hand side of Eq. (I.4) is given by

$$\begin{aligned}
 \int_{-\infty}^{\infty} f^0(v_i - u_i)(v_j - u_j)dv &= \int_{-\infty}^{\infty} \frac{n}{(2\pi\theta)^{3/2}} e^{-(v-u)^2/2\theta} (v_i - u_i)(v_j - u_j)dv \\
 &= \frac{n}{(2\pi\theta)^{3/2}} \int_{-\infty}^{\infty} e^{-(v_1-u_1)^2/2\theta} (v_i - u_i)(v_j - u_j)dv_1 \int_{-\infty}^{\infty} e^{-(v_2-u_2)^2/2\theta} dv_2 \int_{-\infty}^{\infty} e^{-(v_3-u_3)^2/2\theta} dv_3 \\
 &= \frac{n}{(2\pi\theta)^{3/2}} I_1 \times I_2 \times I_3,
 \end{aligned} \tag{I.8}$$

where  $i$  and  $j$  both can take values 1, 2, 3.

For  $i = 1$  and  $j = 1$ ,

$$I_1 = \int_{-\infty}^{\infty} e^{-(v_1-u_1)^2/2\theta} (v_1 - u_1)^2 dv_1.$$

Let  $t = v_1 - u_1 \implies dt = dv_1$

So,

$$\begin{aligned}
 I_1 &= \int_{-\infty}^{\infty} t^2 e^{-t^2/2\theta} dt = \frac{\sqrt{\pi}}{2} (2\theta)^{3/2}, \\
 &\left( \int_{-\infty}^{\infty} x^2 e^{-ax^2} dx = \frac{\sqrt{\pi}}{2} a^{-3/2} \right)
 \end{aligned}$$

$$I_2 = \sqrt{2\pi\theta},$$

$$I_3 = \sqrt{2\pi\theta}.$$

Similarly for  $i = 2$  and  $j = 2$ , (including  $(v_2 - u_2)^2$  in  $I_2$  term)

$$I_1 = \sqrt{2\pi\theta},$$

$$I_2 = \frac{\sqrt{\pi}}{2} (2\theta)^{\frac{3}{2}},$$

$$I_3 = \sqrt{2\pi\theta}.$$

and for  $i = 3$  and  $j = 3$ , (including  $(v_3 - u_3)^2$  in  $I_3$  term)

$$I_1 = \sqrt{2\pi\theta},$$

$$I_2 = \sqrt{2\pi\theta},$$

$$I_3 = \frac{\sqrt{\pi}}{2} (2\theta)^{\frac{3}{2}}.$$

So, for any  $i = j$ , we can say that

$$\begin{aligned} I_1 \times I_2 \times I_3 &= \sqrt{2\pi\theta} \times \sqrt{2\pi\theta} \times \frac{\sqrt{\pi}}{2} (2\theta)^{3/2} \\ \Rightarrow I_1 \times I_2 \times I_3 &= \theta \times (2\pi\theta)^{3/2} \end{aligned} \quad (\text{I.9})$$

For  $i = 1$  and  $j = 2$ ,

$$\begin{aligned} I_1 &= \int_{-\infty}^{\infty} e^{-\frac{(v_1-u_1)^2}{2\theta}} (v_2 - u_2)(v_1 - u_1) dv_1 \\ &= (v_2 - u_2) \int_{-\infty}^{\infty} e^{-\frac{(v_1-u_1)^2}{2\theta}} (v_1 - u_1) dv_1 \\ &= 0 \end{aligned} \quad (\text{I.10})$$

Similarly, it can be said that for any  $i \neq j$ , at least one of the integral will be zero. So,

$$I_1 \times I_2 \times I_3 = 0$$

From Eq.(I.9) and Eq.(I.10) we can say that

$$I_1 \times I_2 \times I_3 = \theta \times (2\pi\theta)^{3/2} \delta_{ij}.$$

where  $\delta_{ij}$  = Kronecker delta.

So, LHS of Eq.(I.4)

$$\begin{aligned} \int_{-\infty}^{\infty} f^0(v_i - u_i)(v_j - u_j) dv &= \frac{n}{(2\pi\theta)^{3/2}} \times \theta \times (2\pi\theta)^{3/2} \delta_{ij} \\ &= n\theta \delta_{ij}. \end{aligned}$$

#### .4 Proof of Eq. (I.5)

Left hand side of Eq.(I.5) is given as

$$\begin{aligned} &\int_{-\infty}^{\infty} f^0(v_i - u_i)(v_j - u_j)(v_\gamma - u_\gamma) dv \\ &= \frac{n}{(2\pi\theta)^{3/2}} \int_{-\infty}^{\infty} e^{-(v-u)^2/2\theta} (v_i - u_i)(v_j - u_j)(v_\gamma - u_\gamma) dv \\ &= \frac{n}{(2\pi\theta)^{3/2}} \int_{-\infty}^{\infty} e^{-(v_1-u_1)^2/2\theta} (v_i - u_i)(v_j - u_j)(v_\gamma - u_\gamma) dv_1 \\ &\quad \int_{-\infty}^{\infty} e^{-(v_2-u_2)^2/2\theta} dv_2 \int_{-\infty}^{\infty} e^{-(v_3-u_3)^2/2\theta} dv_3 \\ &= \frac{n}{(2\pi\theta)^{3/2}} I_1 \times I_2 \times I_3, \end{aligned}$$

For  $i = 1, j = 1$  and  $\gamma = 1$ , we have

$$I_1 = \int_{-\infty}^{\infty} (v_1 - u_1)^3 e^{-(v_1 - u_1)^2 / 2\theta} dv_1.$$

Let  $t = v_1 - u_1 \implies dt = dv_1$

So,

$$I_1 = \int_{-\infty}^{\infty} t^3 e^{-t^2 / 2\theta} dt = 0.$$

For any set of values of  $i, j$ , and  $\gamma$  we can group together the term in  $I_1, I_2$  and  $I_3$  in such a way that at least one of them will be zero. So, for any set of values of  $i, j$ , and  $\gamma$ ,

$$I_1 \times I_2 \times I_3 = 0.$$

So, LHS of Eq.(I.5)

$$\int_{-\infty}^{\infty} f^0(v_i - u_i)(v_j - u_j)(v_\gamma - u_\gamma) dv = 0.$$

## .5 Proof of Eq. (I.6)

Left hand side of Eq.(I.6) is given as

$$\begin{aligned} & \int_{-\infty}^{\infty} f^0(v_i - u_i)(v_j - u_j)(v - u)^2 dv \\ &= \frac{n}{(2\pi\theta)^{3/2}} \int_{-\infty}^{\infty} e^{-(v-u)^2 / 2\theta} (v_i - u_i)(v_j - u_j)(v - u)^2 dv \\ &= \frac{n}{(2\pi\theta)^{3/2}} \int_{-\infty}^{\infty} e^{-(v_1 - u_1)^2 / 2\theta} e^{-(v_2 - u_2)^2 / 2\theta} e^{-(v_3 - u_3)^2 / 2\theta} (v_i - u_i)(v_j - u_j) \left[ (v_1 - u_1)^2 + (v_2 - u_2)^2 + (v_3 - u_3)^2 \right] dv \end{aligned} \quad (\text{I.11})$$

For  $i = 1$  and  $j = 1$ , the above integral becomes

$$\frac{n}{(2\pi\theta)^{3/2}} \int_{-\infty}^{\infty} e^{-(v_1 - u_1)^2 / 2\theta} e^{-(v_2 - u_2)^2 / 2\theta} e^{-(v_3 - u_3)^2 / 2\theta} (v_1 - u_1)^2 \left[ (v_1 - u_1)^2 + (v_2 - u_2)^2 + (v_3 - u_3)^2 \right] dv$$

Let  $v_1 - u_1 = x, v_2 - u_2 = y, v_3 - u_3 = z$

By making the above substitution, we can write the above integral as

$$\frac{n}{(2\pi\theta)^{3/2}} \int_{-\infty}^{\infty} e^{-x^2 / 2\theta} e^{-y^2 / 2\theta} e^{-z^2 / 2\theta} x^2 (x^2 + y^2 + z^2) dx dy dz$$

$$\begin{aligned}
&= \frac{n}{(2\pi\theta)^{3/2}} \left[ \left( \int_{-\infty}^{\infty} x^4 e^{-x^2/2\theta} dx \int_{-\infty}^{\infty} e^{-y^2/2\theta} dy \int_{-\infty}^{\infty} e^{-z^2/2\theta} dz \right) \right. \\
&\quad + \left( \int_{-\infty}^{\infty} x^2 e^{-\frac{x^2}{2\theta}} dx \int_{-\infty}^{\infty} y^2 e^{-y^2/2\theta} dy \int_{-\infty}^{\infty} e^{-z^2/2\theta} dz \right) \\
&\quad \left. + \left( \int_{-\infty}^{\infty} x^2 e^{-x^2/2\theta} dx \int_{-\infty}^{\infty} e^{-y^2/2\theta} dy \int_{-\infty}^{\infty} z^2 e^{-z^2/2\theta} dz \right) \right]
\end{aligned} \tag{I.12}$$

$$\begin{aligned}
&= \frac{n}{(2\pi\theta)^{3/2}} \left[ \left( \sqrt{\pi} 3/4 (2\theta)^{5/2} \times \sqrt{2\theta\pi} \times \sqrt{2\theta\pi} \right) \right. \\
&\quad + \left( \frac{\sqrt{\pi}}{2} (2\theta)^{3/2} \times \frac{\sqrt{\pi}}{2} (2\theta)^{3/2} \times \sqrt{2\theta\pi} \right) \\
&\quad \left. + \left( \frac{\sqrt{\pi}}{2} (2\theta)^{3/2} \times \sqrt{2\theta\pi} \times \frac{\sqrt{\pi}}{2} (2\theta)^{3/2} \right) \right]
\end{aligned} \tag{I.13}$$

$$\begin{aligned}
&= \frac{n}{(2\pi\theta)^{3/2}} \left[ \left( 2\pi\theta \times \sqrt{\pi} \frac{3}{4} (2\theta)^{5/2} \right) + \left( 2 \times (2\theta)^3 \times \sqrt{2\theta\pi} \right) \right] \\
&= \frac{n}{(2\pi\theta)^{3/2}} \times (2\theta)^{7/2} \times \left( \frac{3}{4} \pi^{3/2} + \frac{2}{4} \pi^{3/2} \right) = n(2\theta)^2 \times 5/4 = 5n\theta^2.
\end{aligned} \tag{I.14}$$

We can obtain the same result for  $i = 2; j = 2$  and  $i = 3; j = 3$ , by grouping together the terms in appropriate integrals.

So, for any  $i = j$ , LHS of Eq.(I.6) =  $5n\theta^2$ .

But for any  $i \neq j$ , for example  $i = 1, j = 2$

LHS of Eq.(I.6)

$$= \frac{n}{(2\pi\theta)^{3/2}} \int_{-\infty}^{\infty} e^{-\frac{(v_1-u_1)^2}{2\theta}} e^{-\frac{(v_2-u_2)^2}{2\theta}} e^{-\frac{(v_3-u_3)^2}{2\theta}} \left[ (v_1-u_1)^2 + (v_2-u_2)^2 + (v_3-u_3)^2 \right] (v_1-u_1)(v_2-u_2)$$

Let  $v_1 - u_1 = x, v_2 - u_2 = y, v_3 - u_3 = z$

So,

$$\begin{aligned}
&= \frac{n}{(2\pi\theta)^{3/2}} \left[ \int_{-\infty}^{\infty} (x^2 + y^2 + z^2) xy \left( e^{-x^2/2\theta} \times e^{-y^2/2\theta} \times e^{-z^2/2\theta} \right) \right] \\
&= \frac{n}{(2\pi\theta)^{3/2}} \left[ \left( \int_{-\infty}^{\infty} x^3 e^{-x^2/2\theta} dx \int_{-\infty}^{\infty} ye^{-y^2/2\theta} dy \int_{-\infty}^{\infty} e^{-z^2/2\theta} dz \right) \right. \\
&\quad + \left( \int_{-\infty}^{\infty} xe^{-x^2/2\theta} dx \int_{-\infty}^{\infty} y^3 e^{-y^2/2\theta} dy \int_{-\infty}^{\infty} e^{-z^2/2\theta} dz \right) \\
&\quad \left. + \left( \int_{-\infty}^{\infty} xe^{-x^2/2\theta} dx \int_{-\infty}^{\infty} ye^{-y^2/2\theta} dy \int_{-\infty}^{\infty} ze^{-z^2/2\theta} dz \right) \right] \\
&= \frac{n}{(2\pi\theta)^{3/2}} (0 + 0 + 0) = 0
\end{aligned} \tag{I.15}$$

So, for any  $i \neq j$ , LHS of Eq.(I.6) = 0.

Thus, we can say that

$$\int_{-\infty}^{\infty} f^0(v_i - u_i)(v_j - u_j)(v - u)^2 = 5n\theta^2 \delta_{ij}.$$

where  $\delta_{ij}$  is kroneckor delta.

## A Moments of Maxwell-Boltzmann equilibrium distribution function

### A.1 Zeroth moment of equilibrium distribution function

Zeroth moment of equilibrium distribution function is given by Eq. (I.2) which we have proved in the previous section.

### A.2 First moment of equilibrium distribution function

First velocity moment of equilibrium distribution function is

$$\int_{-\infty}^{\infty} f^0 v_i = nu_i.$$

To prove this we start from Eq. (I.3) (which we have proved in the previous section) i.e.

$$\begin{aligned} \int_{-\infty}^{\infty} f^0(v_i - u_i) &= 0 \\ \Rightarrow \int_{-\infty}^{\infty} f^0 v_i - \int_{-\infty}^{\infty} f^0 u_i &= 0 \\ \Rightarrow \int_{-\infty}^{\infty} f^0 v_i &= u_i \int_{-\infty}^{\infty} f^0 \\ \Rightarrow \int_{-\infty}^{\infty} f^0 v_i &= nu_i \end{aligned} \tag{I.16}$$

### A.3 Second moment of equilibrium distribution function

Second velocity moment of equilibrium distribution function is

$$\int_{-\infty}^{\infty} f^0 v_i v_j = n u_i u_j + n \theta \delta_{ij}.$$

To prove this we start from Eq. (I.4) (which we have proved in the previous section) i.e.

$$\begin{aligned} & \int_{-\infty}^{\infty} f^0 (v_i - u_i)(v_j - u_j) = n \theta \delta_{ij} \\ \Rightarrow & \int_{-\infty}^{\infty} f^0 v_i v_j - \int_{-\infty}^{\infty} f^0 v_i u_j - \int_{-\infty}^{\infty} f^0 u_i v_j + \int_{-\infty}^{\infty} f^0 u_i u_j = n \theta \delta_{ij} \\ \Rightarrow & \int_{-\infty}^{\infty} f^0 v_i v_j - u_j \int_{-\infty}^{\infty} f^0 v_i - u_i \int_{-\infty}^{\infty} f^0 v_j + u_i u_j \int_{-\infty}^{\infty} f^0 = n \theta \delta_{ij} \\ \Rightarrow & \int_{-\infty}^{\infty} f^0 v_i v_j - n u_i u_j - n u_i u_j + n u_i u_j = n \theta \delta_{ij} \\ \Rightarrow & \int_{-\infty}^{\infty} f^0 v_i v_j = n u_i u_j + n \theta \delta_{ij} \end{aligned} \tag{I.17}$$

### A.4 Third moment of equilibrium distribution function

Third velocity moment of equilibrium distribution function is

$$\int_{-\infty}^{\infty} f^0 v_i v_j v_\gamma = n \theta (u_i \delta_{j\gamma} + u_j \delta_{i\gamma} + u_\gamma \delta_{ij}) + n u_i u_j u_\gamma.$$

To prove this we start from Eq. (I.5) (which we have proved in the previous section) i.e.

$$\int_{-\infty}^{\infty} f^0 (v_i - u_i)(v_j - u_j)(v_\gamma - u_\gamma) = 0$$

$$\begin{aligned}
& \Rightarrow \int_{-\infty}^{\infty} f^0 (v_i v_j - v_i u_j - u_i v_j + u_i u_j) (v_\gamma - u_\gamma) = 0 \\
& \Rightarrow \int_{-\infty}^{\infty} f^0 v_i v_j v_\gamma - \int_{-\infty}^{\infty} f^0 v_i u_j v_\gamma - \int_{-\infty}^{\infty} f^0 u_i v_j v_\gamma + \int_{-\infty}^{\infty} f^0 u_i u_j v_\gamma \\
& - \int_{-\infty}^{\infty} f^0 v_i v_j u_\gamma + \int_{-\infty}^{\infty} f^0 v_i u_j u_\gamma + \int_{-\infty}^{\infty} f^0 u_i v_j u_\gamma - \int_{-\infty}^{\infty} f^0 u_i u_j u_\gamma = 0 \\
& \Rightarrow \int_{-\infty}^{\infty} f^0 v_i v_j v_\gamma - u_j \int_{-\infty}^{\infty} f^0 v_i v_\gamma - u_i \int_{-\infty}^{\infty} f^0 v_j v_\gamma + u_i u_j \int_{-\infty}^{\infty} f^0 v_\gamma \\
& - u_\gamma \int_{-\infty}^{\infty} f^0 v_i v_j + u_j u_\gamma \int_{-\infty}^{\infty} f^0 v_i + u_i u_\gamma \int_{-\infty}^{\infty} f^0 v_j - u_i u_j u_\gamma \int_{-\infty}^{\infty} f^0 = 0 \\
& \Rightarrow \int_{-\infty}^{\infty} f^0 v_i v_j v_\gamma - u_j (n u_i u_\gamma + n \theta \delta_{i\gamma}) - u_i (n u_j u_\gamma + n \theta \delta_{j\gamma}) + u_i u_j (n u_\gamma) \\
& \quad - u_\gamma (n u_i u_j + n \theta \delta_{ij}) + u_i u_\gamma (n u_j) + u_j u_\gamma (n u_i) - n u_i u_j u_\gamma = 0 \\
& \Rightarrow \int_{-\infty}^{\infty} f^0 v_i v_j v_\gamma - n u_j \theta \delta_{i\gamma} - n u_i u_j u_\gamma - n u_i \theta \delta_{j\gamma} - n u_\gamma \theta \delta_{ij} = 0 \\
& \Rightarrow \int_{-\infty}^{\infty} f^0 v_i v_j v_\gamma = n u_i u_j u_\gamma + n \theta (u_i \delta_{j\gamma} + u_j \delta_{i\gamma} + u_\gamma \delta_{ij}) \tag{I.18}
\end{aligned}$$

## B Conservation of mass

Boltzmann equation with BGK approximation for collision operator can be written as

$$\partial_t f + v_i \partial_i f + F \partial_v f = \frac{1}{\tau} (f^0 - f). \tag{I.19}$$

Integrating, we get

$$\begin{aligned}
& \int \partial_t f \, dv + \int v_i \partial_i f \, dv + \int F \partial_v f \, dv = \int \frac{1}{\tau} (f^0 - f) \, dv \\
& \Rightarrow \partial_t \int f \, dv + \partial_i \int v_i f \, dv + \partial_v \int F f \, dv = \int \frac{1}{\tau} (f^0 - f) \, dv \\
& \Rightarrow \partial_t n + \partial_i (n u_i) + F \partial_v n = \frac{1}{\tau} (n - n) \\
& \Rightarrow \partial_t n + \partial_i (n u_i) = 0 \tag{I.20}
\end{aligned}$$

## C Conservation of momentum

From Eq. (I.19), we can write

$$f = f^0 - \tau (\partial_t f + v_i \partial_i f + F \partial_v f). \tag{I.21}$$

Eq. (I.19) can be re-written as

$$\partial_t f + v_j \partial_j f + F_j \partial_{v_j} f = \frac{1}{\tau} (f^0 - f).$$

multiplying “ $v_i$ ” on both sides of the above equation and integrating, we get

$$\begin{aligned} \int v_i \partial_t f \, dv + \int v_i v_j \partial_j f \, dv + \int F_j v_i \partial_{v_j} f \, dv &= \int \frac{1}{\tau} (f^0 v_i - f v_i) \, dv \\ \Rightarrow \partial_t \int v_i f \, dv + \partial_j \int v_i v_j f \, dv + F_j \int v_i \partial_{v_j} f \, dv &= \frac{1}{\tau} \int (f^0 v_i - f v_i) \, dv \\ \Rightarrow \partial_t \int v_i f \, dv + \partial_j \int v_i v_j f \, dv + F_j \int v_i \partial_{v_j} f \, dv &= \frac{1}{\tau} (n u_i - n u_i) \\ \Rightarrow \partial_t \int v_i f \, dv + \partial_j \int v_i v_j f \, dv + F_j \int v_i \partial_{v_j} f \, dv &= 0 \end{aligned} \quad (\text{I.22})$$

Now, we simplify each term of Eq. (I.22) one by one.

Third term of left hand side of Eq. (I.22) is

$$\begin{aligned} F_j \int v_i \partial_{v_j} f \, dv &= F_j \left[ v_i \int \partial_{v_j} f \, dv - \int \left( \int \partial_{v_j} f \, dv \right) dv \right] \\ &= F_j \left[ v_i \partial_{v_j} \int f \, dv - \int (\partial_{v_j} \int f \, dv) dv \right] \\ &= F_j (v_i \partial_{v_j} n - \int f \, dv) \\ &= F_j (0 - n) \\ &= -n F_j \end{aligned} \quad (\text{I.23})$$

Substituting Eq. (I.23) in Eq. (I.22), we get

$$\begin{aligned} \partial_t \int v_i f \, dv + \partial_j \int v_i v_j f \, dv - n F_j &= 0 \\ \Rightarrow \partial_t (n u_i) + \partial_j \int v_i v_j f \, dv - n F_j &= 0 \end{aligned} \quad (\text{I.24})$$

Eq. (I.21) can be re-written as

$$f = f^0 - \tau (\partial_t f + v_j \partial_j f + F_j \partial_{v_j} f).$$

multiplying “ $v_i v_j$ ” with all the terms of the above equation and integrating, we get

$$\int f v_i v_j \, dv = \int f^0 v_i v_j \, dv - \tau \left[ \int v_i v_j \partial_t f \, dv + \int v_i v_j v_j \partial_j f \, dv + F_j \int v_i v_j \partial_{v_j} f \, dv \right] \quad (\text{I.25})$$



If we evaluate Eq. (I.25) upto first order in derivative (by doing Taylor series expansion around the equilibrium point) and substitute it in Eq. I.22 we will get Euler equation.

Up to first order in derivative,

$$\begin{aligned} \int f v_i v_j dv &= \int f^0 v_i v_j dv \\ \Rightarrow \int f v_i v_j dv &= n u_i u_j + n \theta \delta_{ij} \end{aligned} \quad (\text{I.26})$$

Substituting Eq. (I.26) in Eq. (I.24), we get

$$\begin{aligned} \partial_t(nu_i) + \partial_j(nu_i u_j + n\theta \delta_{ij}) - nF_i &= 0 \\ \Rightarrow \partial_t(nu_i) + \partial_j(nu_i u_j) &= nF_i - \partial_j(n\theta \delta_{ij}) \end{aligned} \quad (\text{I.27})$$

where Kronecker delta,  $\delta_{ij}$ , is given as

$$\delta_{ij} = \begin{cases} 1, & i = j \\ 0, & i \neq j. \end{cases} \quad (\text{I.28})$$

So, we can write Eq. (I.27) as

$$\partial_t(nu_i) + \partial_j(nu_i u_j) = nF_i - \partial_i(n\theta) \quad (\text{I.29})$$

$$\begin{aligned} \Rightarrow u_i \partial_t n + n \partial_t u_i + u_i \partial_j(nu_j) + nu_j \partial_j u_i &= nF_i - \partial_i(n\theta) \\ \Rightarrow u_i(\partial_t n + \partial_j(nu_j)) + n \partial_t u_i + nu_j \partial_j u_i &= nF_i - \partial_i(n\theta) \end{aligned} \quad (\text{I.30})$$

The bracketed term of left hand side of Eq. (I.30) is zero by equation of continuity(Eq. (I.20)). So, Eq. (I.30) can be written as

$$\partial_t u_i + u_j \partial_j u_i = F_i - \frac{1}{n} \partial_i(n\theta). \quad (\text{I.31})$$

We will use Eqs. (I.30) and (I.31) when we will derive Eq. (I.23) up to second order in derivative and then we will substitute that in Eq. (I.24). That will give us the Navier Stokes equation. So, we have to evaluate three more terms of Eq. (I.25).

Force term in Eq. (I.25) is

$$\begin{aligned} F_\gamma \int v_i v_j \partial_{v_\gamma} f dv &= F_\gamma \left[ v_i v_j \left( \int \partial_{v_\gamma} f dv \right) - \int (v_i v_j)' \left( \int \partial_{v_\gamma} f dv \right) \right] \\ &= F_\gamma \left[ v_i v_j \partial_{v_\gamma} \left( \int f dv \right) - \int (v_i + v_j) \left( \int \partial_{v_\gamma} f dv \right) \right] \\ &= F_\gamma \left[ v_i v_j \partial_{v_\gamma} n - \int (v_j + v_i) f dv \right] \\ &= F_\gamma (-nu_j - nu_i) \\ &= -nF_i u_j - nF_j u_i \end{aligned} \quad (\text{I.32})$$

Substituting Eq. (I.32) in Eq. (I.25), we get

$$\int f v_i v_j dv = \int f^0 v_i v_j dv - \tau \left[ \partial_t \int f^0 v_i v_j dv + \partial_\gamma \int f^0 v_i v_j v_\gamma dv - n F_i u_j - n F_j u_i \right] \quad (\text{I.33})$$

While obtaining Eq. (I.33) from Eq. (I.25), we have also made the following approximation

$$\begin{aligned} \partial_t \int f v_i v_j dv &\approx \partial_t \int f^0 v_i v_j dv, \\ \partial_\gamma \int f v_i v_j v_\gamma dv &\approx \partial_\gamma \int f^0 v_i v_j v_\gamma dv. \end{aligned}$$

The time derivative term of Eq. (I.33) can be simplify as

$$\begin{aligned} \partial_t \left( \int f^0 v_i v_j dv \right) &= \partial_t (n u_i u_j + n \theta \delta_{ij}) \\ &= u_j \partial_t (n u_i) + n u_i \partial_t u_j + \theta \delta_{ij} \partial_t n + n \partial_t \theta \delta_{ij} \end{aligned} \quad (\text{I.34})$$

From Eq. (I.29), we can say that

$$\partial_t (n u_i) = n F_i - \partial_i (n \theta) - \partial_\gamma (n u_i u_\gamma) \quad (\text{I.35})$$

From Eq. I.31, we can say that

$$\partial_t u_j = F_j - \frac{1}{n} \partial_j (n \theta) - u_\gamma \partial_\gamma u_j \quad (\text{I.36})$$

From equation of continuity(Eq. I.20), we can say that

$$\partial_t n = -\partial_\gamma (n u_\gamma) \quad (\text{I.37})$$

and we use the relation

$$\partial_t \theta = -u_\gamma \partial_\gamma \theta - \frac{2}{3} \partial_\gamma (\theta u_\gamma) \quad (\text{I.38})$$

We have used the above relation directly but this can also be derived from by multiplying  $(v - u)^2$  with Eq. (I.22). Substituting Eqs. (I.35), (I.36), (I.37) and (I.38) in Eq. (I.34), we get

$$\begin{aligned} \partial_t \left( \int f^0 v_i v_j dv \right) &= u_j \left[ n F_i - \partial_i (n \theta) - \partial_\gamma (n u_i u_\gamma) \right] + n u_i \left[ F_j - \frac{1}{n} \partial_j (n \theta) - u_\gamma \partial_\gamma u_j \right] \\ &\quad + \theta \delta_{ij} (-\partial_\gamma (n u_\gamma)) + n \delta_{ij} \left[ -u_\gamma \partial_\gamma \theta - \frac{2}{3} \partial_\gamma (\theta u_\gamma) \right] \end{aligned} \quad (\text{I.39})$$

The space derivative term in Eq. (I.33) can be simplified as

$$\begin{aligned}
\partial_\gamma \int f^0 v_i v_j v_\gamma dv &= \partial_\gamma \left[ n\theta(u_i \delta_{j\gamma} + u_j \delta_{i\gamma} + u_\gamma \delta_{ij}) + nu_i u_j u_\gamma \right] \\
&= \partial_\gamma(n\theta u_i \delta_{j\gamma}) + \partial_\gamma(n\theta u_j \delta_{i\gamma}) + \partial_\gamma(n\theta u_\gamma \delta_{ij}) + \partial_\gamma(nu_i u_j u_\gamma) \\
&= \partial_j(n\theta u_i) + \partial_i(n\theta u_j) + \partial_\gamma(n\theta u_\gamma \delta_{ij}) + \partial_\gamma(nu_i u_j u_\gamma)
\end{aligned} \tag{I.40}$$

Adding Eqs. (I.39) and (I.40), we get

$$\begin{aligned}
\partial_t \left( \int f^0 v_i v_j dv \right) + \partial_\gamma \int f^0 v_i v_j v_\gamma dv &= -\partial_\gamma(nu_i u_j u_\gamma) - u_i \partial_j(n\theta) - u_j \partial_i(n\theta) \\
&\quad + n(F_i u_j + F_j u_i) - \delta_{ij} \partial_\gamma(nu_\gamma \theta) - \frac{2}{3} n \delta_{ij} \partial_\gamma(\theta u_\gamma) \\
&\quad + \partial_j(n\theta u_i) + \partial_i(n\theta u_j) + \partial_\gamma(n\theta u_\gamma \delta_{ij}) + \partial_\gamma(nu_i u_j u_\gamma) \\
&= n\theta \partial_j(u_i) + n\theta \partial_i(u_j) + n(F_i u_j + F_j u_i) - \frac{2}{3} n \delta_{ij} \partial_\gamma(\theta u_\gamma)
\end{aligned} \tag{I.41}$$

Substituting Eq. (I.41) in Eq. (I.33), we get

$$\begin{aligned}
\partial_t \int f v_i v_j dv &= nu_i u_j + n\theta \delta_{ij} \\
&\quad - \tau \left[ n\theta(\partial_j u_i + \partial_i u_j) + n(F_i u_j + F_j u_i) - \frac{2}{3} n \delta_{ij} \partial_\gamma(u_\gamma \theta) - nF_i u_j - nF_j u_i \right] \\
&\Rightarrow \int f v_i v_j dv = nu_i u_j + n\theta \delta_{ij} - n\theta \tau \left( \partial_j u_i + \partial_i u_j - \frac{2}{3} \delta_{ij} \partial_\gamma(u_\gamma) \right) \\
&\Rightarrow \int f v_i v_j dv = nu_i u_j + n\theta \delta_{ij} - \eta \left( \partial_j u_i + \partial_i u_j - \frac{2}{3} \delta_{ij} \partial_\gamma(u_\gamma) \right)
\end{aligned} \tag{I.42}$$

where  $\eta = n\theta\tau$ .

Now, substituting Eq. (I.42) in Eq. (I.25), we get

$$\begin{aligned}
\partial_t(nu_i) + \partial_j \left[ nu_i u_j + n\theta \delta_{ij} - \eta \left( \partial_j u_i + \partial_i u_j - \frac{2}{3} \delta_{ij} \partial_\gamma(u_\gamma) \right) \right] - nF_i &= 0 \\
\Rightarrow \partial_t(nu_i) + \partial_j(nu_i u_j) + \partial_j(n\theta) \delta_{ij} = nF_i + \partial_j \left[ \eta \left( \partial_j u_i + \partial_i u_j - \frac{2}{3} \delta_{ij} \partial_\gamma(u_\gamma) \right) \right]
\end{aligned} \tag{I.43}$$

For  $i = j$ ,  $\delta_{ij} = 1$ .

So, Eq. (I.43) can be written as

$$\begin{aligned}
 u_i \partial_t n + n \partial_t (u_i) + u_i \partial_j (n u_j) + n u_j \partial_j u_i &= -\partial_i (n \theta) + n F_i + \partial_j \left[ \eta \left( \partial_j u_i + \partial_i u_j - \frac{2}{3} \delta_{ij} \partial_\gamma (u_\gamma) \right) \right] \\
 \Rightarrow u_i \left( \partial_t n + \partial_j (n u_j) \right) + n \partial_t (u_i) + n u_j \partial_j u_i &= -\partial_i (n \theta) + n F_i + \partial_j \left[ \eta \left( \partial_j u_i + \partial_i u_j - \frac{2}{3} \delta_{ij} \partial_\gamma (u_\gamma) \right) \right]
 \end{aligned} \tag{I.44}$$

Using equation of continuity i.e Eq. (I.20) in the above equation, we get

$$n \partial_t (u_i) + n u_j \partial_j u_i = -\partial_i (n \theta) + n F_i + \partial_j \left[ \eta \left( \partial_j u_i + \partial_i u_j - \frac{2}{3} \delta_{ij} \partial_\gamma (u_\gamma) \right) \right]. \tag{I.45}$$

Eq. (I.45) is the compressible Navier stokes equation in tensor notation.

# Bibliography

- BARBI, C., FAVIER, D., MARESCA, C. & TELIONIS, D. 1986 Vortex shedding and lock-on of a circular cylinder in oscillatory flow. *Journal of Fluid Mechanics* **170**, 527–544.
- BEARMAN, P. W. 1984 Vortex shedding from oscillating bluff bodies. *Annual Review of Fluid Mechanics* **16** (1), 195–222.
- BEHR, M., HASTREITER, D., MITTAL, S. & TEZDUYAR, T. 1995 Incompressible flow past a circular cylinder: dependence of the computed flow field on the location of the lateral boundaries. *Computer Methods in Applied Mechanics and Engineering* **123** (1-4), 309–316.
- BHATNAGAR, P. L., GROSS, E. P. & KROOK, M. 1954 A model for collision process in gases. i. small amplitude processes in charged and neutral one-component system. *Phys. Rev.* **94**, 511.
- BISHOP, R. & HASSAN, A. 1964 The lift and drag forces on a circular cylinder oscillating in a flowing fluid. *Proceedings of the Royal Society of London. Series A. Mathematical and Physical Sciences* **277** (1368), 51–75.
- CARBERRY, J., SHERIDAN, J. & ROCKWELL, D. 2001 Forces and wake modes of an oscillating cylinder. *Journal of Fluids and Structures* **15** (3), 523–532.
- CARNEVALE, G., FUENTES, O. V. & ORLANDI, P. 1997 Inviscid dipole-vortex rebound from a wall or coast. *Journal of Fluid Mechanics* **351**, 75–103.
- CETINER, O. & ROCKWELL, D. 2001 Streamwise oscillations of a cylinder in a steady current. part 1. locked-on states of vortex formation and loading. *Journal of Fluid Mechanics* **427**, 1–28.
- DIPANKAR, A., SENGUPTA, T. & TALLA, S. 2007 Suppression of vortex shedding behind a circular cylinder by another control cylinder at low reynolds numbers. *Journal of Fluid Mechanics* **573**, 171–190.
- DIXIT, H. & BABU, V. 2006 Simulation of high rayleigh number natural convection in a square cavity using the lattice boltzmann method. *International journal of heat and mass transfer* **49** (3), 727–739.
- DUTTA, S., PANIGRAHI, P. & MURALIDHAR, K. 2007 Sensitivity of a square cylinder wake to forced oscillations. *Journal of fluids engineering* **129** (7), 852–870.

- GOLDSTEIN, S. & ROSENHEAD, L. 1936 Boundary layer growth. In *Proc. Camb. Phil. Soc.*, vol. 32, pp. 392–401. Cambridge Univ Press.
- GRIFFIN, O. M. 1971 The unsteady wake of an oscillating cylinder at low reynolds number. *Journal of Applied Mechanics* **38** (4), 729–738.
- GRIFFIN, O. M. & RAMBERG, S. E. 1976 Vortex shedding from a cylinder vibrating in line with an incident uniform flow. *Journal of Fluid Mechanics* **75** (02), 257–271.
- HOMANN, F. 1936 Der einfluss grosser zähigkeit bei der strömung um den zylinder und um die kugel. *ZAMM-Journal of Applied Mathematics and Mechanics/Zeitschrift für Angewandte Mathematik und Mechanik* **16** (3), 153–164.
- KHALEDI, H. A., ANDERSSON, H. I., BARRI, M. & PETTERSEN, B. 2012 Flow past a normal flat plate undergoing inline oscillations. *Physics of Fluids (1994-present)* **24** (9), 093603.
- KONSTANTINIDIS, E. & BALABANI, S. 2007 Symmetric vortex shedding in the near wake of a circular cylinder due to streamwise perturbations. *Journal of Fluids and Structures* **23** (7), 1047–1063.
- KONSTANTINIDIS, E., BALABANI, S. & YIANNESKIS, M. 2005 The timing of vortex shedding in a cylinder wake imposed by periodic inflow perturbations. *Journal of Fluid Mechanics* **543**, 45–55.
- KOVASZNAY, L. 1949 Hot-wire investigation of the wake behind cylinders at low reynolds numbers. *Proceedings of the Royal Society of London. Series A. Mathematical and Physical Sciences* **198** (1053), 174–190.
- KRISHNAMOORTHY, S., PRICE, S. & PAIDOUSSIS, M. 2001 Cross-flow past an oscillating circular cylinder: synchronization phenomena in the near wake. *Journal of Fluids and Structures* **15** (7), 955–980.
- LEE, T. & BUDWIG, R. 1991 A study of the effect of aspect ratio on vortex shedding behind circular cylinders. *Physics of Fluids A: Fluid Dynamics (1989-1993)* **3** (2), 309–315.
- LEONTINI, J. S., LO JACONO, D. & THOMPSON, M. C. 2011 A numerical study of an inline oscillating cylinder in a free stream. *Journal of Fluid Mechanics* **688**, 551.
- MITTAL, S. & KUMAR, B. 2003 Flow past a rotating cylinder. *Journal of Fluid Mechanics* **476**, 303–334.
- MURALIDHAR, P., FERRER, N., DANIELLO, R. & ROTHSTEIN, J. P. 2011 Influence of slip on the flow past superhydrophobic circular cylinders. *J. Fluid Mech* **680**, 459–476.
- NISI, H. & PORTER, A. W. 1923 On eddies in air. *The London, Edinburgh, and Dublin Philosophical Magazine and Journal of Science* **46** (275), 754–768.
- OBASAJU, E. 1983 An investigation of the effects of incidence on the flow around a square section cylinder. *Aeronautical quarterly* **34**, 243–259.

- OERTEL JR, H. 1990 Wakes behind blunt bodies. *Annual Review of Fluid Mechanics* **22** (1), 539–562.
- OKAJIMA, A. 1982 Strouhal numbers of rectangular cylinders. *Journal of Fluid Mechanics* **123**, 379–398.
- ONGOREN, A. & ROCKWELL, D. 1988 Flow structure from an oscillating cylinder. 2. mode competition in the near wake. *Journal of Fluid Mechanics* **191**, 225–245.
- PARKINSON, G. 1989 Phenomena and modelling of flow-induced vibrations of bluff bodies. *Progress in Aerospace Sciences* **26** (2), 169–224.
- PERDIKARIS, P. G., KAIKTSIS, L. & TRIANTAFYLLOU, G. S. 2009 Chaos in a cylinder wake due to forcing at the strouhal frequency. *Physics of Fluids (1994-present)* **21** (10), 101705.
- PRANDTL, L. 1925 The magnus effect and windpowered ships. *Naturwissenschaften* **13**, 93–108.
- ROSHKO, A. 1954 On the development of turbulent wakes from vortex streets .
- SAJJAD, M. & SOHN, C. 2014 Numerical study of flow past a square cylinder with corner curvature at incidence. In *Applied Sciences and Technology (IBCAST), 2014 11th International Bhurban Conference on*, pp. 294–297. IEEE.
- SEN, S., MITTAL, S. & BISWAS, G. 2009 Steady separated flow past a circular cylinder at low reynolds numbers. *Journal of Fluid Mechanics* **620**, 89–119.
- SRIKANTH, T., DIXIT, H. N., TATAVARTI, R. & GOVINDARAJAN, R. 2011 Vortex shedding patterns, their competition, and chaos in flow past inline oscillating rectangular cylinders. *Physics of Fluids (1994-present)* **23** (7), 073603.
- STÄGER, R. & ECKELMANN, H. 1991 The effect of endplates on the shedding frequency of circular cylinders in the irregular range. *Physics of Fluids A: Fluid Dynamics (1989-1993)* **3** (9), 2116–2121.
- STRYKOWSKI, P. & SREENIVASAN, K. 1990 On the formation and suppression of vortex shedding at low reynolds numbers. *Journal of Fluid Mechanics* **218**, 71–107.
- TANEDA, S. 1956 Experimental investigation of the wake behind a sphere at low reynolds numbers. *Journal of the Physical Society of Japan* **11** (10), 1104–1108.
- TOKUMARU, P. & DIMOTAKIS, P. 1993 The lift of a cylinder executing rotary motions in a uniform flow. *Journal of Fluid Mechanics* **255**, 1–10.
- TUDBALL-SMITH, D., LEONTINI, J. S., SHERIDAN, J. & JACONO, D. L. 2012 Streamwise forced oscillations of circular and square cylinders. *Physics of Fluids (1994-present)* **24** (11), 111703.
- WILLIAMSON, C. & ROSHKO, A. 1988 Vortex formation in the wake of an oscillating cylinder. *Journal of fluids and structures* **2** (4), 355–381.

XU, S., ZHOU, Y. & WANG, M. 2006 A symmetric binary-vortex street behind a longitudinally oscillating cylinder. *Journal of Fluid Mechanics* **556**, 27–43.

YOKOI, Y. & KAMEMOTO, K. 1994 Vortex shedding from an oscillating circular cylinder in a uniform flow. *Experimental thermal and fluid science* **8** (2), 121–127.

ZDRAVKOVICH, M. & CARELAS, E. 1997 Aerodynamics of a covered pedestrian bridge of a trapezoidal section. *Journal of wind engineering and industrial aerodynamics* **66** (2), 141–153.

ZHOU, C. & GRAHAM, J. 2000 A numerical study of cylinders in waves and currents. *Journal of fluids and structures* **14** (3), 403–428.